

TOPICAL REVIEW

The Gravitational Wave Signature of Core-Collapse Supernovae

Christian D Ott

E-mail: cott@tapir.caltech.edu

Theoretical Astrophysics, Mailcode 130-33,
California Institute of Technology, Pasadena, California 91125, USA
and

Niels Bohr International Academy, Niels Bohr Institute,
Blegdamsvej 17, 2100 Copenhagen, Denmark

Abstract. We review the ensemble of anticipated gravitational-wave (GW) emission processes in stellar core collapse and postbounce core-collapse supernova evolution. We discuss recent progress in the modeling of these processes and summarize most recent GW signal estimates. In addition, we present new results on the GW emission from postbounce convective overturn and protoneutron star g -mode pulsations based on axisymmetric radiation-hydrodynamic calculations. Galactic core-collapse supernovae are very rare events, but within 3–5 Mpc from Earth, the rate jumps to 1 in ~ 2 years. Using the set of currently available theoretical gravitational waveforms, we compute upper-limit optimal signal-to-noise ratios based on current and advanced LIGO/GEO600/VIRGO noise curves for the recent SN 2008bk which exploded at ~ 3.9 Mpc. While initial LIGOs cannot detect GWs emitted by core-collapse events at such a distance, we find that advanced LIGO-class detectors could put significant upper limits on the GW emission strength for such events. We study the potential occurrence of the various GW emission processes in particular supernova explosion scenarios and argue that the GW signatures of neutrino-driven, magneto-rotational, and acoustically-driven core-collapse SNe may be mutually exclusive. We suggest that even initial LIGOs could distinguish these explosion mechanisms based on the detection (or non-detection) of GWs from a galactic core-collapse supernova.

PACS numbers: 97.60.Bw, 97.60.Jd, 97.60.-s, 97.10.Kc, 04.30.Db, 04.40.Dg

1. Introduction

Ever since the very first experimental efforts to detect gravitational waves (GWs), core-collapse supernovae (SNe) have been considered as potential astrophysical emission sites. There are very strong indications from theory and observation that multi-D dynamics play a prominent and probably decisive role in core-collapse SNe (see, e.g., [1, 2]). GWs are emitted at lowest order by an accelerated mass-energy quadrupole moment. Hence, by their intrinsic multi-D nature, GWs, if detected from a core-collapse event, will very likely prove powerful messengers that can provide detailed and live dynamical information on the intricate multi-D dynamics occurring deep inside collapsing massive stars.

Massive stars ($8\text{--}10 M_{\odot} \lesssim M \lesssim 100 M_{\odot}$ at zero-age main sequence [ZAMS]) form electron-degenerate cores composed primarily of iron-group nuclei in the final

stages of their exoergic nuclear burning. Once such an iron core exceeds its effective Chandrasekhar mass (see, e.g., [3, 4]) it grows gravitationally unstable. Collapse ensues, leading to dynamical compression of the inner core material to nuclear densities. There, the nuclear equation of state (EOS) stiffens, resulting in the rebound of the inner core (“core bounce”). A hydrodynamic shock wave is launched at the outer edge of the inner core and propagates outward in mass and radius, slamming into the still infalling outer core. Owing to the dissociation of heavy nuclei and to energy losses to neutrinos that stream away from the postshock region, the shock quickly loses energy, stalls and must be *revived* to plow through the stellar envelope, blow up the star, and produce a SN explosion, leaving behind a neutron star. Without shock revival, black-hole (BH) formation is inevitable and even with a successful explosion, a BH may still form via fall-back accretion.

Iron core collapse is the most energetic process in the modern universe, liberating some 10^{53} erg = 100 B (Bethe) of gravitational energy. Most of this energy, $\sim 99\%$, is emitted in neutrinos as the protoneutron star (PNS) contracts and cools over a timescale of ~ 100 s. Only $\sim 1\%$ goes into the asymptotic energy of the SN explosion and becomes visible in the electromagnetic spectrum. The fundamental question that core-collapse SN theory has been facing for the past ~ 45 years is how exactly the necessary fraction of gravitational energy is transferred to revive the shock and ultimately unbind the stellar envelope. Shock revival must occur sooner than 1–1.5 s after bounce (depending on progenitor star structure setting the rate of mass accretion) in order to produce a compact remnant that obeys observational and theoretical neutron star upper baryonic mass limits around ~ 1.5 – $2.5 M_{\odot}$ (see [5] and references therein).

The SN *explosion mechanism* may involve (a combination of) heating of the postshock region by neutrinos, multi-dimensional hydrodynamic instabilities of the accretion shock, in the postshock region, and in the PNS, rotation, PNS pulsations, magnetic fields, and nuclear burning (for a recent review, see [2], but also [6]). Three SN mechanisms are presently discussed in the literature. The *neutrino mechanism* has the longest pedigree [2, 4, 7], is based on postbounce neutrino energy deposition behind the stalled shock, and appears to require [8, 9, 10] convection and the standing-accretion-shock instability (SASI, see, e.g., [11] and references therein) to function in all but the very lowest-mass massive stars which may explode even in spherical symmetry [12, 13]. Recent detailed 2D neutrino-radiation hydrodynamics simulations by the Garching group produced explosions in particular $11.2 M_{\odot}$ and $15 M_{\odot}$ progenitor models [8, 9]. However, it is not yet clear how the neutrino mechanism’s efficacy varies with progenitor ZAMS mass and structure and what its detailed dependence on the high-density nuclear EOS may be.

The *magneto-rotational (or MHD) mechanism*, probably operating only in the context of rapid progenitor rotation, depends on magnetic-field amplification during collapse and at postbounce times. It leads to explosions that develop in jet-like fashion along the axis of rotation [14, 15, 16, 17, 18] and may reach hypernova energies of ~ 10 B [17]. The MHD mechanism may also be relevant in the context of long-soft gamma-ray bursts (GRBs, see, e.g., [19]) and could be a precursor, setting the stage for a later GRB (e.g., [17], but see [20]).

The *acoustic mechanism* for core-collapse SNe, as recently proposed by Burrows et al. [6, 21, 22, 23], requires the excitation of large-amplitude PNS pulsations (primarily g -modes) by turbulence and SASI-modulated accretion downstreams.

These pulsations damp by the emission of strong sound waves that steepen to shocks and deposit energy in the postshock region, eventually leading to late explosions at $\gtrsim 1$ s after bounce. This mechanism appears to be sufficiently robust to blow up even the most massive and extended progenitors, but has so far not been confirmed by other groups (see also [24, 25]).

Constraining the core-collapse SN mechanism via astronomical observations is difficult. The intricate pre-explosion dynamics of the SN core deep inside the supergiant presupernova star are inaccessible by the traditional means of astronomy. Theoretical models of the SN mechanism can currently be tested via secondary observables only, including the asymptotic explosion energy, ejecta morphology, nucleosynthesis products, compact remnant mass and proper motion, and pulsar spin/magnetic fields.

GWs and neutrinos are the only messengers with the potential of delivering first-hand information on the physical processes leading to explosion: Both are emitted deep inside the SN core and travel to observers on Earth practically without interaction with intervening material.

A small number of neutrinos were detected from SN 1987A in the Large Magellanic (distance $D \approx 50$ kpc; see, e.g., [4] and references therein). GWs have not yet been observed directly, but the advent of GW astronomy has begun. An international network of broad-band light-interferometric GW observatories is active, encompassing the US LIGOs [26], the British-German GEO600 [27], the French-Italian VIRGO [28] and the Japanese TAMA 300 [29]. The three LIGO interferometers have recently reached their design sensitivities, and, in their S5 science run, have taken a year worth of data, partly in coincidence with GEO600 and VIRGO. In addition, there are a number of active resonant bar/sphere GW detectors in operation, including the four bar detectors of the International Gravitational Event Collaboration (IGEC-2), ALLEGRO, AURIGA, EXPLORER, and NAUTILUS [30], and the resonant spheres MiniGrail [31] and Schenberg [32]. The current status of ground-based GW detection was recently summarized by Whitcomb [33].

GWs from astrophysical sources are weak and notoriously difficult to detect (e.g., [34]). Hence, in order to disentangle an astrophysical GW signal from the mostly overwhelming detector noise, GW astronomy does not only require sensitive detectors, but also extensive processing and analysis of the detector output on the basis of reliable theoretical estimates for the GW signals presently expected from astrophysical sources. The latter must, in most cases, be obtained via detailed numerical modeling of the dynamics responsible for the GW emission in a given source.

In iron core collapse and postbounce SN evolution, the emission of GWs is expected primarily from rotating collapse and bounce, nonaxisymmetric rotational instabilities, postbounce convective overturn/SASI, and PNS pulsations. In addition, anisotropic neutrino emission, global precollapse asymmetries in the iron core and surrounding burning shells, aspherical mass ejection, magnetic stresses, and the late-time formation of a black hole may contribute to the overall GW signature.

The aim of this topical review is to summarize the recent significant progress in the modeling of the various GW emission processes in core-collapse SNe with a focus on the early postbounce, pre-explosion SN evolution up to $\sim 1 - 2$ seconds after bounce. We do not cover the GW emission from the collapse of supermassive primordial or very massive population III stars, dynamical fission processes, late-time fall-back accretion on black holes, nuclear phase-transitions in PNSs, or from late-time

postbounce secular instabilities such as r -modes. Other reviews of the GW signature of core-collapse SNe are those of Kotake et al. [35] and Fryer and New [36].

In section 2, we provide a concise historical overview on early work and go on to discuss computational core-collapse SN modeling and the various ways in which GR and GW extraction are treated in section 3. Section 4 covers the most extensively modeled GW emission mechanism, rotating core collapse and bounce. The potential for and the GW emission from nonaxisymmetric rotational instabilities is the topic of section 5. Section 6 is devoted to the emission of GWs from convective overturn and SASI, while we discuss the GW signal from PNS core pulsations in section 7. To both of these sections we add new, previously unpublished results obtained via 2D Newtonian radiation-hydrodynamics calculations. In section 8, we discuss the emission of GWs from anisotropic neutrino radiation fields and in section 9 we summarize the GW signals associated with rapid aspherical outflows, precollapse global asymmetries, strong magnetic stresses, and PNS collapse to a black hole.

While the SN rate in the Milky Way and the local group of galaxies is rather low and probably less than 1 SN per two decades (e.g., [37]), there may be 1 SN occurring about every other year between 3 – 5 Mpc from Earth [38]. The recent SN 2008bk, which exploded roughly 3.9 Mpc away, is an example SN from this region of space. Thus, in section 10, we present optimal single-detector matched-filtering signal-to-noise ratios for LIGO/GEO600/VIRGO and advanced LIGOs for a subset of the gravitational waveforms reviewed in this article and with an assumed source distance corresponding to that of SN 2008bk. We find that initial LIGO-class detectors had no chance of detecting GWs from SN 2008bk. Advanced LIGOs, however, could put some constraints on the GW emission strength, but still would probably not allow detailed GW observations. We wrap up our review in section 11 with a critical summary of the subject matter and discuss in which way the various GW emission processes can be linked to particular SN explosion mechanisms. We argue that the GW signatures of the neutrino, MHD, and acoustic SN mechanisms may be mutually exclusive and that the mere detection, or, in fact non-detection, of GWs from a nearby core-collapse SN can constrain significantly the core-collapse SN explosion mechanism.

In this review article, all values of the dimensionless GW signal amplitudes h_+ and h_\times are given for optimal source-observer orientation and a source distance of 10 kpc is typically assumed. In most figures showing GW signals, the waveforms are plotted as $h_{+, \times} D$, rescaled by distance D and in units of centimeters. Summaries of GW extraction methods can be found in [34, 39, 40, 41, 42] and a comparison of Newtonian and general relativistic methods were presented in [43, 44].

2. A Short Overview on Early Work

Although gravitational waves were proposed by Einstein himself in 1918 [45], there was general disagreement on the waves' reality and their ability to carry off energy from their source until a 1957 gedankenexperiment by Bondi [46] restored trust in the fundamental theory of GWs (see, e.g., [34] and references therein for more details). This led to a renaissance of GW physics in the early to mid 1960s, resulting in much theoretical work on astrophysical sites of GW emission (see, e.g., [34, 47]) and to the first experimental searches for GWs led by Weber with resonant bar detectors [33, 48].

GW emission in the core-collapse SN context first appeared in a 1966 paper by Weber [49] in which he referred to unpublished work from 1962 by Dyson [50]

on astrophysical sources of GWs, including binary neutron star systems and non-spherical stellar collapse[‡]. Also in 1966, Wheeler, based on unpublished work by Zee and himself, published first quantitative estimates of the emission of a GW burst by quadrupole oscillations of a PNS associated with core bounce [52]. In the following years, the theory of NS pulsations and their GW emission characteristics was worked out by Thorne, Bardeen, Meltzer, and collaborators [53, 54, 55, 56, 57, 58, 59], leading to many subsequent studies and opening up a rich independent branch of research (see, e.g., [60, 61] for reviews).

In their 1971 review [51], Ruffini and Wheeler provided a first comprehensive summary of scenarios for GW emission in the stellar collapse context and provided quantitative estimates for the GW signal from rotating core collapse and bounce, (early postbounce) neutron star pulsations, and nonaxisymmetric neutron star deformations.

A number of subsequent studies in the 1970s and early 1980s focussed on aspherical collapse and relied upon semi-analytical descriptions of collapsing and/or oscillating homogeneous spheroids and ellipsoids. Key studies were those carried out by Thuan and Ostriker [62], Novikov [63], Shapiro [64], Saenz and Shapiro [65, 66, 67], Epstein [68], Moncrief [69], and Detweiler and Lindblom [70]. Most of these early and ground-breaking investigations severely overestimated the strength (amplitude/energy) of the GW burst from core collapse and bounce and failed to capture the qualitative features of the core bounce GW burst observed later in numerical simulations. Some of the former and other authors using similar techniques also studied the GW emission from nonaxisymmetric rotational deformations of rapidly rotating postbounce neutron stars [67, 71, 72, 73, 74, 75].

In 1979, Turner and Wagoner [76] followed a different approach and used perturbation theory to calculate the GW emission produced by rotationally-induced perturbations of spherically symmetric numerical iron core collapse models of Van Riper [77] and Wilson [78]. Seidel and collaborators followed along those lines and perturbatively analyzed detailed spherically-symmetric general-relativistic (GR) core collapse simulations in the 1980s [79, 80]. Although the perturbative approach is in principle appropriate only for small deviations from sphericity and, hence, for very slowly rotating stellar cores, the GW signals from core bounce predicted by Seidel et al. is in rough qualitative agreement with the signals obtained from more recent multi-D simulations of even rapidly rotating stellar cores.

Epstein [81] and independently Turner [82] considered in their 1978 studies the GW emission from anisotropic neutrino emission in stellar core collapse and developed the linear-theory formalism that has since been applied to extract GWs from aspherical neutrino radiation fields in multi-D radiation-hydrodynamic simulations.

The early epoch of work on the GW emission in stellar core collapse was dominated by analytic, semi-analytic, and perturbative studies, largely because of a lack of computers sufficiently powerful to carry out multi-D numerical non-linear hydrodynamics simulations. The end of this epoch was marked by the emergence of the first supercomputers and their general availability to the astrophysics community beginning in the late 1970s and early 1980s.

[‡] Upon being asked by the author to comment on his early work on GW emission from stellar collapse, Dyson wrote: *I have no idea who first calculated the emission of gravitational radiation from a collapsing star with rotation. Ruffini and Wheeler [51] may have been the first. It was certainly obvious to everyone who thought about it that a collapsing star with rotation would give rise to a strong pulse of gravitational waves. I make no claim to have thought of this first.* F. Dyson, priv. comm., Oct. 2006.

3. Modeling Core-Collapse Supernovae

The Einstein equations as well as the equations of radiation-magnetohydrodynamics are families of coupled non-linear partial differential equations for which solutions can be found analytically only in very few limiting cases, leaving numerical modeling as the only viable route to their solution in complex scenarios such as stellar collapse and core-collapse SNe. Hence, for an accurate understanding of the core-collapse SN phenomenon and the GW signals emitted by the involved multi-D dynamics, detailed numerical models are required.

Modeling stellar core collapse and the postbounce evolution of the SN core is a multi-scale multi-physics problem that involves lengthscales from the extended pre-SN stellar core (thousands of kilometers) down to small-scale turbulence in the postbounce flow (on the order of meters) and timescales from $\lesssim 10^{-6}$ s (the typical computational timestep) to up to 1 – 2 s (the time for the development of a full explosion or for BH formation to occur).

An ideal and complete (“realistic”) model should resolve all lengthscales, should be free of artificially imposed symmetries (i.e., be 3D) and should fully include general relativity, GR MHD, multi-D GR Boltzmann neutrino transport, and a microphysical treatment of EOS and nuclear and neutrino interactions. In addition, since the high-density EOS, the pre-SN stellar structure and angular momentum configuration are not well constrained, extensive parameter studies are necessary to plow the parameter space of possible EOS and pre-SN configurations. Present-day 2D core-collapse SN simulations, e.g., those carried out by [9, 17, 22, 83], scale to ~ 48 -128 compute cores and typically require multiple months to complete on current supercomputers. A single 3D full GR radiation-(magneto)hydrodynamics simulation will have an at least a 100 times (and more realistically, 1000 to 10000 times) greater computational complexity and will need to scale to thousands of compute cores on next-generation supercomputers to complete within reasonable time§.

None of the currently published numerical models of core collapse and postbounce SN evolution live up to the above standards and all studies employ approximations for multiple of the physical ingredients listed. A detailed discussion of the various approximations cannot be provided here, but since the focus of this review is on GWs, a consequence of GR and, in principle, requiring a full GR treatment, we present in the following the different ways in which GR gravity, relativistic dynamics, and GW extraction from matter and spacetime dynamics are presently handled in multi-D core-collapse simulations.

- (i) **Newtonian gravity and dynamics.** Many recent multi-D simulations (e.g., [17, 21, 22, 23, 41, 83, 85, 86, 87, 88, 89, 90]) employ a solution of the Newtonian Poisson equation for computing the gravitational acceleration terms and treat (magneto)-hydrodynamics and radiation transport (if included) in Newtonian fashion. GWs are extracted from the fluid motions via the slow-motion, weak-field quadrupole formalism (e.g., [34, 91, 92]).
- (ii) **Approximate GR gravity.** Motivated by the work of the Garching SN group [93, 94, 95], a set of recent core-collapse SN simulations [8, 9, 96, 97, 98] take GR into account via replacing the spherical component of the multipole decomposition of the Newtonian gravitational potential with an effective GR

§ See [84] for a more quantitative discussion of the computational complexity of the core-collapse SN problem.

potential modeled after the Tolman-Oppenheimer-Volkoff (TOV) potential (e.g., [99]). The hydrodynamics, however, are treated in standard Newtonian fashion. Redshift and time-dilation effects are taken into account in the radiation transport sector in the simulations of the Garching SN group [8, 95]. GWs are extracted via the slow-motion, weak-field quadrupole formalism [34, 91, 92].

- (iii) **Conformally-flat (CFC) GR.** In the conformally-flat (or conformal-flatness condition [CFC]) approximation to GR introduced by Isenberg [100] and first used by Wilson et al. [101], the general 3-metric of the 3 + 1 decomposition (e.g., [102]) is replaced by the flat-space Minkowski metric scaled with a conformal-factor ϕ^4 . The CFC approximation is exact in spherical symmetry. In multi-D, a CFC spacetime behaves as an approximation of GR at first post-Newtonian order [103] and may be regarded as GR minus the dynamical degrees of freedom of the gravitational field that correspond to the GW content at infinity. However, even stationary spacetimes without GWs can be non-CFC, e.g., rotating NSs or Kerr BHs (e.g., [104, 105]). An extension of the CFC approach with terms of second post-Newtonian order, CFC+, was introduced by Cerdá-Durán and collaborators [106]. The CFC approximation permits the use of the full GR (M)HD equations (e.g., [107]) and is employed in simulations of axisymmetric rotating core collapse by Dimmelmeier and collaborators [108, 109, 110, 111, 112, 113, 114]. At least for this scenario it has been shown to be an excellent approximation to full GR [106, 115]. Since a CFC spacetime does not contain GWs, they must be extracted from the fluid dynamics via variants of the slow-motion, weak-field quadrupole formalism, making use of the conserved variables of GR (M)HD (e.g., [108, 112]).
- (iv) **Full GR.** Multi-D simulations in full 2 + 1 and 3 + 1 GR evolve the Einstein equations without approximations and with appropriate choices of temporal and spatial gauge (e.g., [102]). Full GR simulations of rotating core collapse and early postbounce evolution were carried out by Shibata et al. [116, 117, 118] and by Ott et al. [42, 115, 119] who employed the BSSN spacetime evolution system [102, 120, 121]. In principle, GWs can be extracted directly from the spacetime in regions sufficiently far away from the emission region (e.g., [122] and references therein). Due to the relative weakness of the GWs emitted in core collapse, the direct extraction has proven to be numerically difficult and most studies resort to the same slow-motion, weak-field quadrupole formalism used in the CFC context||.

Studies addressing the GW signature of stellar core collapse and core-collapse SNe historically followed two general approaches.

One approach focussed on the detailed treatment of EOS, microphysics and radiation transport as necessary for physically accurate models of the collapse and postbounce phase. Studies following this approach were either Newtonian or employed approximate GR, neglecting the additional complication of CFC or full GR (e.g., [23, 39, 86, 87, 97, 123, 124]). Due to the large computational complexity (dominated by neutrino transport) of such detailed simulations, these studies were limited to small model sets and, hence, were unable to cover the parameter space of possible initial configurations and EOS.

Studies following the second approach were primarily concerned with the GW signal of rotating core collapse and bounce. Their emphasis was on performing large

|| See [43, 44] for comparisons of gauge-invariant extraction techniques with variants of the quadrupole formalism.

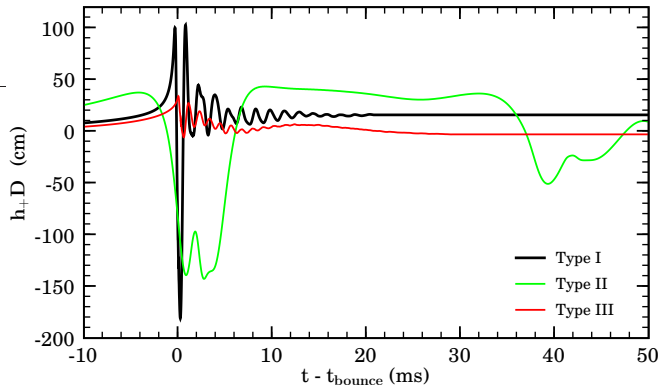


Figure 1. Axisymmetric GW burst signal ($h_+ D$ in units of cm, where D is the distance of the source) as a function of time after core bounce for models A1B3G3 (type I), A2B4G1 (type II), and A1B3G5 (type III) of the 2002 GR study using polytropic initial models and a simple analytic hybrid polytropic/ideal-fluid EOS carried out by Dimmellemeier et al. [112]. The waveforms were obtained from [126].

parameter studies of precollapse rotational configurations in Newtonian gravity, CFC, or full GR and, in some cases, included magnetic fields. Their schemes typically did not take into account a microphysical EOS, detailed neutrino transport and microphysics, and presupernova models from stellar evolutionary calculations (see, e.g., [40, 41, 90, 112, 116, 125], but note that [41] employed a microphysical EOS, but neglected deleptonization).

Only recently, these two approaches have begun to come together in the first extensive CFC and full GR parameter studies of rotating core collapse with a microphysical EOS and an approximate deleptonization scheme carried out by Dimmellemeier et al. [108, 109] and Ott et al. [42, 115, 119]. The results of these studies will be discussed extensively in the following section.

4. Rotating Core Collapse and Bounce

Rapid precollapse rotation, in combination with angular momentum conservation during collapse, leads to significant asphericity in the form of a GW emitting, rapidly time-varying $\ell = 2$ oblate (quadrupole) deformation of the collapsing and bouncing core.

Rotating collapse and core bounce is the most extensively studied GW emission process in the massive star collapse context. In 1982, Müller published in [127] the first GW signals from rotating core collapse and bounce that were based on the axisymmetric (2D) Newtonian simulations of Müller and Hillebrandt [128]. A large number of 2D studies followed with varying degrees of microphysical detail, inclusion of GR, and precollapse model sets (see, e.g., [39, 40, 41, 86, 112, 116, 129] and references therein). These computational parameter studies demonstrated that the general analytic picture of stellar core collapse derived by Goldreich & Weber [130] and Yahil [131] for spherically-symmetric collapse also holds to good approximation for rotating cores: From the beginning of collapse, the collapsing core separates into a subsonically homologously ($v \propto r$) contracting *inner core* and a supersonically infalling

outer core. The mass of the inner core at core bounce sets the mass cut for the matter that is dynamically relevant in bounce (see, e.g., [4]) and responsible for the GW burst. It also determines the initial size of the PNS.

Furthermore, these studies identified at least three GW signal “types” that can be associated with distinctly different types of collapse and bounce dynamics (figure 1 displays representative examples). Type I models undergo core bounce governed by the stiffening of the nuclear EOS at nuclear density and “ring down” quickly into postbounce equilibrium. Their waveforms exhibit one pronounced large spike at bounce and then show a gradually damped ring down. Type II models, on the other hand, are affected significantly by rotation and undergo core bounce dominated by centrifugal forces at densities below nuclear. Their dynamics exhibits multiple slow harmonic-oscillator-like damped bounce–re-expansion–collapse cycles (“multiple bounces”), which is reflected in the waveform by distinct signal peaks associated with every bounce. It is interesting to note that type-II models are related to *fizzlers*, proposed (e.g., [132, 133, 134]) collapse events of self-gravitating fluid bodies that become temporally or permanently stabilized by centrifugal forces before core bounce or black-hole formation.

Type III models are characterized by fast collapse (owing to a very soft subnuclear EOS or very efficient electron capture), extremely small masses of the homologously collapsing inner core, and low-amplitude GW emission and a subdominant negative spike in the waveform associated with bounce.

GWs from collapse with magnetic fields were studied by [87, 90, 96, 117, 125] who found an additional dynamics/signal type IV which occurs only in the case of very strong precollapse core magnetization ($B \gtrsim 10^{12}$ G). Such strong precollapse magnetic fields are unlikely to occur in nature and the aforementioned studies showed that weaker magnetic fields have little dynamical consequence during collapse and bounce (see also the discussion in [17]). However, MHD-driven jet-like bipolar outflows and time-changing magnetic fields themselves can lead to the emission of GWs (see the discussion in section 9)

Recently, Ott et al. [115, 119] and Dimmelmeier et al. [108, 109] presented the first 3D full GR and 2D CFC GR simulations of rotating stellar collapse that incorporate GR as well as a microphysical finite-temperature nuclear EOS and an approximate scheme by Liebendörfer (first presented in [139]) to account for electron capture and neutrino losses during collapse. These calculations for the first time included all the known most relevant physics in the collapse and bounce phase and, in the case of [108], also considered two different nuclear EOS, the Lattimer-Swesty EOS [140] and the Shen EOS [135, 136].

The results of Dimmelmeier et al. [108] show that the combined effects of deleptonization and GR decrease the mass and extent of the homologous inner core and reduce significantly the relevance of centrifugal support for a large set of progenitor models and a wide range of precollapse rotational configurations. This set encompasses and goes beyond what is deemed realistic in the context of collapsing massive stars (see, e.g., [141, 142]). In particular, they find that the GW signal of rotating collapse and core bounce is of generic Type-I shape. Type-II dynamics with the associated “multiple bounce” GW signals do not obtain when GR and deleptonization are included. Type-III dynamics are also absent, since they require very efficient electron capture and resulting very small masses of the inner core $\lesssim 0.3 M_{\odot}$ that do not occur in the iron core collapse context where the smallest inner core mass is $\gtrsim 0.45 M_{\odot}$ [108].

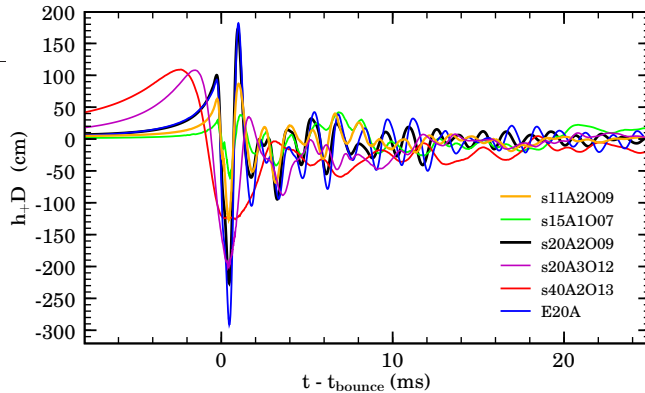


Figure 2. GW signals ($h_+ D$ in units of cm, where D is the distance of the source) for a few examples from the 2D GR model set of Dimmelmeier et al. [108]. The models shown here were computed with the Shen EOS [135, 136] and employ 1D presupernova models of [137], spanning the progenitor mass range from $11.2 M_\odot$ (s11) to $40 M_\odot$ (s40). The models were set up with precollapse central angular velocities $\Omega_{c,i}$ from $\sim 1.5 \text{ rad s}^{-1}$ to $\sim 11 \text{ rad s}^{-1}$. For details of the rotational setup, see [108]. Model E20A uses a $20\text{-}M_\odot$ presupernova model that was evolved by [138] with a 1D prescription for rotation. Note the generic shape of the waveforms, exhibiting one pronounced spike at core bounce and a subsequent ring down. Very rapid precollapse rotation ($\Omega_{c,i} \gtrsim 6 \text{ rad s}^{-1}$; models s20A3O12 and s40A2O13 in this plot) results in a significant slow-down of core bounce, leading to a lower-amplitude and lower-frequency GW burst. The GW signal data are available for download from [126].

Table 1. Summary of the GW signal characteristics of rotating iron core collapse and core bounce based on the waveforms of Dimmelmeier et al. [108]. All models exhibit type-I dynamics and waveform morphology and can be organized into three distinct groups based primarily on their precollapse central angular velocity $\Omega_{c,i}$. $|h_{\text{max}}|$ is the maximum gravitational wave strain amplitude (scaled to 10 kpc) at bounce, E_{GW} is the energy radiated away in gravitational waves, f_{peak} is the frequency at which the GW energy spectrum dE_{GW}/df peaks, and Δf_{50} is the frequency interval centered about f_{peak} that contains 50% of E_{GW} . Note that f_{max} used by Dimmelmeier et al. is the peak of the GW signal spectrum and not the peak of dE_{GW}/df . Also note that for the slowly rotating group prompt postbounce convective overturn contributes significantly to the overall GW signal. The convective contribution was removed from the waveforms before analysis, since the deleptonization scheme employed by Dimmelmeier et al. and Ott et al. is ineffective at postbounce times and is likely to overestimate the strength and duration of prompt convection after bounce [108].

Group	$\Omega_{c,i}$ (rad s^{-1})	$ h_{\text{max}} $ (10^{-21} at 10 kpc)	E_{GW} ($10^{-8} M_\odot c^2$)	f_{peak} (Hz)	Δf_{50} (Hz)
1	$\lesssim 1\text{--}1.5$	$\lesssim 0.5$	$\lesssim 0.1$	$\sim 700\text{--}800$	~ 400
2	$1\text{--}2$ to $6\text{--}13$	0.5 to 10	0.1 to 5	$\sim 400\text{--}800$ most models: $700\text{--}800$	100 to 400
3	$\gtrsim 6\text{--}13$	3.5 to 7.5	0.07 to 0.5	70 to 200	80 to 250

Furthermore, Dimmelmeier et al. [108] demonstrate that the rotating collapse and bounce dynamics and the resulting GW burst signal depend primarily on the precollapse central angular velocity $\Omega_{c,i}$ and secondarily on the progenitor mass, which influences precollapse iron core entropy and mass, which, in turn affects the mass of the inner core at bounce (see, e.g., [3, 143]). The degree of differential rotation and the stiffness of the particular choice of nuclear EOS appear to have little influence on the general characteristics of the GW signal.

Figure 2 shows example waveforms of a subset of the models considered by Dimmelmeier et al. [108] whose waveform data are available from [126]. Although all models exhibit generic type-I dynamics and signal morphology, the dynamics and GW signals can be ordered into three groups (for more details, see [108] and the summary in table 1):

- (1) Slowly rotating iron cores with $\Omega_{c,i} \lesssim 1\text{--}1.5 \text{ rad s}^{-1}$ undergo core bounce dominated by nuclear pressure effects, develop only a small quadrupole deformation and yield small peak GW amplitudes $|h_{\text{max}}|$ at core bounce that are generally below $\sim 5 \times 10^{-22}$ for a galactic core-collapse event at 10 kpc distance. All slowly rotating models exhibit strong prompt postbounce convective overturn in the postshock region owing to the negative entropy gradient left behind by the stalling the shock. Because of the lack of postbounce neutrino transport, the strength and duration of the prompt convection is probably overestimated in these models [108] (see also section 6.1 in this article).
- (2) Moderately rapidly to rapidly rotating iron cores with $1\text{--}2 \text{ rad s}^{-1} \lesssim \Omega_{c,i} \lesssim 6\text{--}13 \text{ rad s}^{-1}$ still experience pressure-dominated bounce, but develop larger quadrupole deformations and have a rotationally increased mass of the inner core at bounce. This results in sizeable peak GW amplitudes and energy emissions (see table 1). Prompt postbounce convection is suppressed by positive specific angular momentum gradients in the postshock region and does not contribute to the GW signal (see, e.g., [141]). The upper end of the range in $\Omega_{c,i}$ for this group is dependent on progenitor characteristics. Progenitors with massive (and higher-entropy) iron cores tend to transition to the next group at lower $\Omega_{c,i}$. Dimmelmeier et al. find approximate transition $\Omega_{c,i}$ of $\gtrsim 13$, ~ 9 , ~ 11 , and $\sim 7 \text{ rad s}^{-1}$ for their 11.2, 15, 20, and 40 M_{\odot} models, respectively.
- (3) Very rapid precollapse rotation ($\Omega_{c,i} \gtrsim 6\text{--}13 \text{ rad s}^{-1}$; the actual value depending on the progenitor model) results in slow core bounce governed exclusively by centrifugal forces at significantly subnuclear densities. This results in a decrease of $|h_{\text{max}}|$ and a shift of the peak of the GW energy spectrum to frequencies below $\sim 400 \text{ Hz}$.

Figure 3 contrasts the strengths of the GW bursts of the models of Dimmelmeier et al. [108] with initial LIGO sensitivity [26]. Plotted is the initial LIGO dimensionless rms strain sensitivity $h_{\text{rms}} = \sqrt{fS(f)}$ as a function of frequency f , where $S(f)$ is the noise spectral density in units of $(\text{Hz})^{-1/2}$. Each dot represents a particular model and is plotted at that model's detector-dependent characteristic GW frequency f_c and characteristic strain h_c , computed by Dimmelmeier et al. according to the prescription given in [34]. The models cluster in the h_c - f_c plane according to their membership in one of the three groups discussed above. Slowly rotating models (group 1) have small h_c and moderately high f_c . With increasing $\Omega_{i,c}$, the model move upward and slightly to the right (higher h_c and slightly higher f_c). Moderately

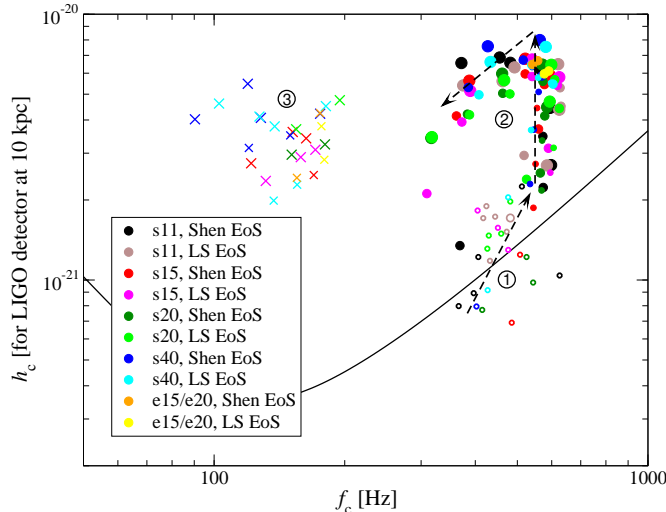


Figure 3. Location of the GW signals of Dimmelmeier et al. [108] in the h_c - f_c plane (using the detector-dependent definitions of h_c and f_c given in [34]) relative to the $h_{\text{rms}} = \sqrt{fS(f)}$ sensitivity of initial LIGO and for a source distance of 10 kpc. The three groups of signals discussed in the text and summarized in table 1 are marked. This plot is similar to figure 16 of [108] and based on freely available data [126].

rapid models (group 2) reach high h_c and cluster in f_c between 600 and 800 Hz. The most rapidly rotating models of that group move somewhat to the left in f_c , while very rapidly rotating and centrifugally bouncing models (group 3) cluster at low f_c and lower h_c , but still exhibit a high signal to noise ratio (SNR) with initial LIGO and at a distance of 10 kpc. Hence, according to figure 3, GWs from moderately rapidly to rapidly rotating core collapse and bounce within the Milky Way should be detectable by current LIGO-class detectors. In addition, it may be possible, based on a determination of the dominant emission frequency (ideally in combination with a determination of the progenitor mass by other astronomical means), to constrain the precollapse iron core rotation.

To conclude this section, we point out that according to the most recent stellar evolutionary models and pulsar birth spin estimates [141, 142], garden-variety massive stars at solar metallicity are probably spinning with central angular velocities significantly below 1 rad s^{-1} (group 1). GW bursts from core bounce of such models are unlikely to be detectable by current detectors and may be marginally detectable by advanced LIGO. More rapid rotation may be relevant in the context of gamma-ray burst progenitors (see, e.g., [19]) which could make up perhaps $\sim 1\%$ of the single massive star population, but may occur primarily at low metallicities [144].

5. Rotational Nonaxisymmetric Instabilities

From the classical theory of Newtonian MacLaurin spheroids (see, e.g., [145, 146]) one finds that rotating axisymmetric fluid bodies become unstable to nonaxisymmetric deformations due to a dynamical instability at rotation rates $\beta = T/|W| \gtrsim 0.27 \equiv \beta_{\text{dyn}}$, where T is the rotational kinetic and $|W|$ the gravitational energy of the spheroid.

A secular (dissipation driven[‡]) instability may set in at $\beta = T/|W| \gtrsim 0.14 \equiv \beta_{\text{sec}}$, though, due to its secular nature, has longer growth times than the dynamical instability.

Stars that go unstable to the classical MacLaurin-type dynamical or secular instability develop global azimuthal (nonaxisymmetric) structure that, at least in the linear regime, can be characterized in terms of modes m with spatial structure proportional to $\exp(im\varphi)$, where φ is the azimuthal angle. In most cases the bar-like $m = 2$ mode is dominant and one frequently speaks of a “bar mode instability”. Direct numerical simulations have demonstrated (e.g., [147, 148, 149]) that β_{dyn} holds approximately even in the case of differentially rotating compressible fluid configurations in GR. For the secular instability, perturbative studies suggest an onset at significantly lower β in GR (see, e.g., [61, 146] for discussions). However, GR hydrodynamic studies of the secular instability remain yet to be carried out.

A spinning bar is a simple system that emits GWs at twice its rotational frequency (due to its π -symmetry) with amplitudes $|h_{\text{bar}}| \propto MR^2\Omega^2/D$, where M is the bar’s mass, $2R$ its length, and $\Omega = 2\pi f$ its angular velocity. Using the Newtonian quadrupole approximation, one can derive an estimate for the GW amplitude [88],

$$|h_{\text{bar}}| \approx 4.5 \times 10^{-21} \left(\frac{\epsilon}{0.1}\right) \left(\frac{f}{500 \text{ Hz}}\right)^2 \times \left(\frac{D}{10 \text{ kpc}}\right)^{-1} \left(\frac{M}{0.7 M_{\odot}}\right) \left(\frac{R}{12 \text{ km}}\right)^2, \quad (1)$$

where ϵ is the ellipticity of the bar. The scaling of (1) is set up to reflect a PNS core of $0.7 M_{\odot}$ with a 2 ms period and a radius of 12 km that is deformed only moderately ($\epsilon = 0.1$) and located at a distance of 10 kpc.

5.1. Instability at High- β

The literature on nonaxisymmetric instabilities in rotating fluid bodies is extensive and cannot be reviewed here in the necessary detail. Relatively recent reviews and relevant references can be found in [61, 146, 148]. In the context of massive star collapse and PNSs, the first Newtonian 3D simulations were carried out by Rampp et al. [150] and Brown [151] who followed the postbounce development of nonaxisymmetric dynamics in extremely differentially and rapidly rotating simplified stellar models that reached up to $\beta \approx 0.35$ at bounce in 2D and were mapped to 3D shortly before or after bounce. With a similar approach, though in full GR, Shibata & Sekiguchi [118] studied the development of nonaxisymmetric dynamics in models that reached β near β_{dyn} and reported the development of $m = 2$ and $m = 1$ dynamics in their models.

Ott et al. [115, 119, 141] and very recently Dimmelmeier et al. [108] studied via their 3D full GR and 2D CFC GR core-collapse simulations the prospects for nonaxisymmetric rotational instabilities in massive star collapse and postbounce evolution. Their models included microphysical details and they considered a large number of precollapse rotational configurations that covered a parameter space, encompassing and going beyond current predictions from stellar evolution theory and constraints from pulsar birth spin estimates [141, 142, 144].

Ott et al. and Dimmelmeier et al. found that even their most extreme models do not reach values of β close to β_{dyn} during collapse, bounce, and during early

[‡] Possible mechanisms are physical viscosity and gravitational-wave reaction. See, e.g., [61, 146].

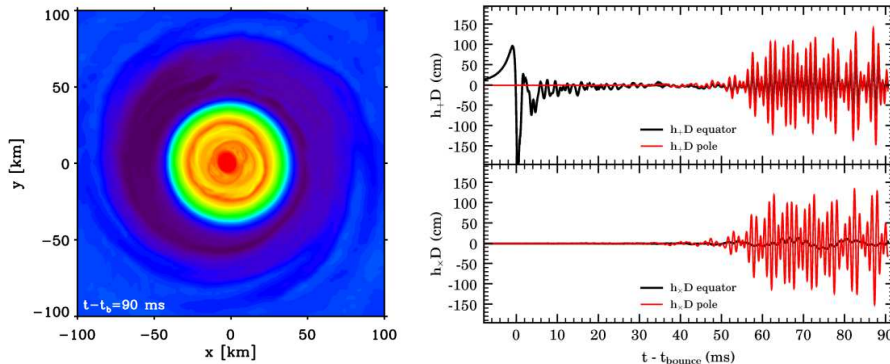


Figure 4. **Left:** Colormap depicting the specific entropy distribution in the equatorial plane of the $20-M_{\odot}$ model s20A2B4 of Ott et al. [42, 115, 119] at 90 ms after core bounce. Red and yellow regions of the PNS core have low entropy ($\sim 1\text{--}3$ k_{B} /baryon) while dark blue and black symbolize high entropy > 6 k_{B} /baryon. The nonaxisymmetric structures are of primarily $m = \{1, 2, 3\}$ nature with radial variations in dominance. **Right:** GW polarizations h_+ (top panel) and h_{\times} (bottom panel) multiplied by distance D as seen by observers along the equator (black) and along the pole (red) in the same model. Significant nonaxisymmetric dynamics with $m = 2$ components develop around 30–40 ms after core bounce at a rotation rate $\beta \sim 0.13$. Note that the GW burst signal from core bounce is purely axisymmetric, since an axisymmetric system has vanishing h_{\times} and vanishing GW emission along the axis of symmetry. The waveforms are available from [155].

postbounce times. Their work confirmed results obtained in studies considering evolutionary sequences of rotating PNSs [152] and 2D Newtonian simulations [41, 141].

On the basis of the current understanding, it appears rather unlikely that a PNS in nature develops a high- β rotational instability before, at, or early after bounce. As the PNS contracts and cools on a timescale of seconds to minutes and if angular momentum is conserved and not redistributed by other means (see, e.g., [17, 117, 141]), it spins up and may reach β_{dyn} . It is, however, more likely that the secular instability driven by viscous dissipation or GW back reaction, which in PNSs has a growth timescale of the order of or larger than ~ 1 s [153, 154], may set in first.

5.2. Instability at Low- β

Via 3D full GR simulations that were carried out self-consistently from the onset of collapse, Ott et al. [42, 115, 119] confirmed that stellar cores with precollapse parameters in the investigated parameter space stay axisymmetric throughout collapse, bounce and the very early postbounce phase. Furthermore, they found the development of nonaxisymmetric dynamics at postbounce times $\gtrsim 20$ ms in a subset of their models. The 3D dynamics were of predominantly $m = \{1, 2, 3\}$ spatial character (see the left panel of figure 4) and were followed to late times in only two models, one having a postbounce β of 0.09, the other one spinning with $\beta \approx 0.13$. Very recently, Scheidegger et al. [96], who performed a 3D Newtonian study with a monopole gravitational potential with relativistic corrections, found a similar instability in a model with a smaller postbounce value of β around 0.04–0.05.

The instability at low- β seen in simulations may be related to a class of co-rotation dynamical shear instabilities that operates on the shear-energy stored in differential rotation and that powers azimuthal modes via resonant coupling with the background fluid. This occurs at co-rotation points where the mode pattern speed coincides with the fluid angular velocity [156, 157]. Such a low- β instability was first observed in a compact-star context by Centrella et al. [158] in 2001 and multiple subsequent studies confirmed its presence in differentially rotating equilibrium stellar models below the classical high- β instability limits (e.g., [159, 160, 161, 162]). In 2005, Ott et al. [163] discovered a low- β instability in a 3D simulation of a simplified postbounce stellar core.

Differential rotation develops naturally in the outer core during stellar collapse [141]. Hence, such low- β instabilities could – in principle – occur in any PNS with (1) angular velocities at the edge of the inner core that are comparable to the pattern speed of unstable modes and (2) with sufficient total rotational energy and strong enough differential rotation to provide power for significant nonaxisymmetric deformation.

The right part of figure 4 depicts the GW signal of a $20-M_{\odot}$ model of Ott et al. [115, 119] that experiences the low- β nonaxisymmetric instability. Shown are the + (top panel) and \times (bottom panel) GW polarizations for observers located along the polar axis (red) and observers located in the equatorial plane at zero azimuth (black). The PNS and postshock region stay axisymmetric through bounce and exhibit GW emission only in the + polarization and away from the poles. The nonaxisymmetric dynamics reach sizable amplitudes around 30–40 ms and their $m = 2$ components emit GWs in bar-like fashion with correlated strong emission in h_+ and h_{\times} that is strongest for observers located perpendicular to the equatorial plane. The simulation on which figure 4 is based was tracked to ~ 90 ms after core bounce, but the instability could potentially continue for hundreds of milliseconds until angular momentum has been redistributed by the instability or by another process (e.g., via the magneto-rotational instability [MRI]; see, e.g., [164, 165] and references therein).

The simple and rough estimate of equation (1) for a slightly deformed PNS core rotating with a period of 2 ms matches the GW signal of the low- β instability shown in figure 4 quite well and other models of Ott et al. and Scheidegger et al. to within a factor of a few. Concretely, these studies found maximum GW signal amplitudes in the range of $\sim 1\text{--}5 \times 10^{-21}$ (at 10 kpc) and total emitted GW energies E_{GW} of $\sim 5\text{--}15 \times 10^{-8} M_{\odot} c^2$. Most of the energy ($> 50\%$) is emitted in a frequency interval of $\Delta f_{50} \approx 50\text{--}200$ Hz about the frequency f_{peak} at which dE_{GW}/df peaks, which is $\sim 900\text{--}940$ Hz in the models of Ott et al. and Scheidegger et al. Comparing the just stated quantitative results with those summarized for rotating collapse and bounce in table 1, one notes that the GW emission due to nonaxisymmetric rotational dynamics does not necessarily dominate in signal amplitude, but does so clearly in total emitted energy. Its E_{GW} scales with the number n of “emission cycles,” which, of course, depends on the duration of the nonaxisymmetric dynamics.

As demonstrated by [96, 115, 119, 163], the potential for a strong enhancement of the GW signature of rotating core collapse by a low- β -type rotational instability is great. However, the number of 3D core-collapse models in which such an instability was observed is still very limited and the systematic dependence on β , degree of differential rotation, and thermodynamic and magneto-hydrodynamic configuration of the PNS remains to be established. Furthermore, it will be necessary to understand the long-term behavior of the instability and its interaction and competition with

other shear instabilities such as the MRI.

6. Postbounce Convection and SASI

Convective instability is a central feature of the postbounce evolution of core-collapse SN and has been discussed extensively (e.g., [2, 8, 21, 22, 89, 166, 167, 168, 169, 170, 171] and references therein). According to the Schwarzschild-Ledoux criterion [172], convective overturn develops in the presence of negative radial entropy or composition gradients (see, e.g., [8, 167]).

Convective overturn in postbounce SN cores is expected as entropy- and lepton-gradient driven *prompt convection* which may occur immediately after bounce, lepton-gradient driven *PNS convection*, and *neutrino-driven convection* in the postshock heating region. Convection will occur at postbounce times in virtually all core-collapse events, but can be weakened and limited to polar regions by positive specific angular momentum gradients in rapidly rotating cores [83, 89, 141, 173].

The standing-accretion-shock instability (SASI; see, e.g., [11, 21, 174, 175, 176] and references therein) is believed to be caused by either an advective-acoustic [11, 174] or a purely acoustic [175, 176] feedback cycle, leading to the growth of perturbations in the stalled shock. In axisymmetry, the dominant SASI modes are of $\ell = \{1, 2\}$ character, while in the largely unexplored 3D case, power may go into azimuthal m modes. This can reduce the saturation amplitudes in the ℓ modes (see [177] for first 3D results, but also [178] for a perturbative analysis without symmetry constraints).

The SASI grows to non-linear amplitudes over a timescale of typically 200–300 ms after bounce with some dependence on initial accretion shock radius, neutrino luminosity, and accretion rate (e.g., [10, 11]). Rapid rotation may delay the growth of the SASI and weaken the overall phenomenon in 2D [83], while favoring azimuthal SASI modes in 3D [178].

Once active at significant amplitudes, the SASI heavily distorts the postshock region, affecting convection to great extent. In addition, it enhances and modulates accretion funnels that appear as kinks in the shock and channel low entropy material at high rates onto the PNS core [21].

Both convection and SASI are intrinsically multi-D phenomena and lead generically to time-varying mass quadrupole moments, hence, emit GWs. The emission of GWs by convection was first considered by Müller and Janka [124] in 2D and 3D postbounce models with an approximate treatment of neutrino heating and cooling. Subsequent studies with more detailed neutrino transport and microphysics were carried out by Müller et al. [97], Fryer et al. [179], Ott et al. [23, 42], and very recently by Marek et al. [98]. Kotake et al. [85] were the first to specifically address GW emission associated with the SASI using a simple neutrino heating/cooling scheme.

In the following, we discuss the GW emission from convection and SASI, present new results that were performed with the VULCAN/2D SN code [22, 41, 180] and contrast them with previous work. VULCAN/2D is an axisymmetric Newtonian multi-group flux-limited diffusion (MGFLD) radiation-hydrodynamics code. It employs an unsplit arbitrary Lagrangian-Eulerian (ALE) scheme that allows for a central pseudo-Cartesian grid that transitions to a polar-type grid at a transition radius (see figure 4 of [41]).

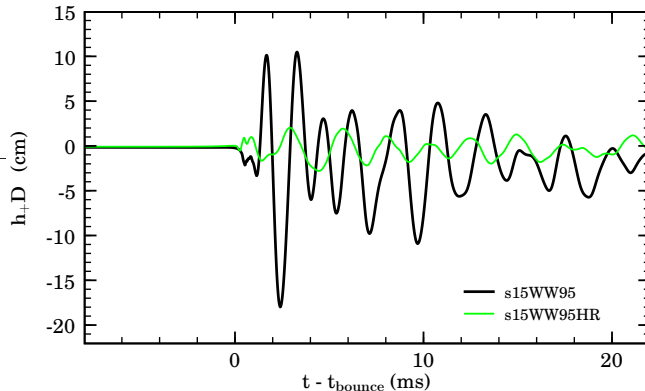


Figure 5. GW burst signal (h_+D in units of cm) due to 2D prompt postbounce convection in a nonrotating $15-M_\odot$ model that employed the precollapse profile of [181]. The model calculations were performed with the VULCAN/2D code [22, 41, 180]. VULCAN/2D uses a central pseudo-Cartesian grid that is matched to a polar-type grid at a transition radius (20 km in s15WW95HR and 30 km in s15WW95). The transition introduces artificial perturbations that act as seeds for prompt convection. Model s15WW95HR is a high-resolution variant of s15WW95 with $\sim 45\%$ more zones in the central region. The resolution – in other words – seed perturbation dependence of prompt convection is apparent. The GW signal data shown here are available from [155].

6.1. Prompt Convection

As the stalling bounce shock passes through outer core material, it leaves behind a negative entropy gradient. Furthermore, following neutrino shock breakout and the associated burst of electron neutrinos (e.g., [8, 171, 182]), a negative lepton gradient arises at the outer edge of the PNS immediately below the neutrinosphere[§]. The two negative gradients lead to a convectively unstable region according to the Schwarzschild-Ledoux criterion [98, 183, 184, 185].

Neutrino losses and, to a limited degree, neutrino energy deposition behind the stalling shock, smooth out the large negative entropy gradient in the immediate postshock region, but prompt convection can still develop rapidly and last for $\gtrsim 10$ –20 ms if significant seed perturbations are present in the immediate postbounce flow [41, 179, 183, 184, 185].

The magnitude and distribution of seed perturbations in the central regions of iron cores in nature is presently unknown. However, it is not unlikely that the late burning stages of stellar evolution result in inhomogeneities in the iron core that do not smooth out completely between the end of core burning and core collapse (see also the discussion of large-scale precollapse asymmetries in section 9.2). Such inhomogeneities are frozen in during collapse and may act as seed perturbations for prompt convection [179, 186, 187].

Here, we present results from VULCAN/2D simulations using a nonrotating $15-M_\odot$ progenitor model of [181]. Model s15WW95 uses the standard simulation setup presented in [22, 23], while model s15WW95HR is set up with 45% higher

[§] The neutrinosphere can be defined as the surface at which the optical depth for neutrinos τ_ν , given by $\tau_\nu = \int_\infty^R dr \lambda_\nu^{-1}$, is equal to $2/3$. Here, λ_ν is the (energy-averaged) neutrino mean-free path. Note that the neutrino sphere is strongly dependent on neutrino energy and species.

radial and angular resolution inside ~ 300 km. The Cartesian–polar transition of the VULCAN/2D grid introduces artificial perturbations that converge away with increasing resolution and decreasing transition radius. These numerical perturbations act as seeds for prompt convection.

Figure 5 depicts the GW signal of prompt convection as seen in the VULCAN/2D simulations. In both calculations, prompt convection is strongest inside a radius of ~ 60 km from the origin. However, one should keep in mind that the region in which prompt convection is most pronounced depends on the location and strength of the negative entropy gradient *and* on the location and magnitude of the seed perturbations. In the standard-resolution variant, the large seed perturbations lead to strong prompt convection and a correspondingly large GW burst setting in within ~ 1 ms of core bounce. The maximum GW amplitude is $\sim 6 \times 10^{-22}$ (at 10 kpc) and within ~ 20 ms, an energy of $\sim 1.5 \times 10^{-10} M_{\odot} c^2$ is emitted in GWs. The peak of the GW energy spectrum is at $f_{\text{peak}} \approx 680$ Hz and 50% of the energy is emitted at frequencies $\delta_{f,50} = 150$ Hz centered about f_{peak} . The higher resolution calculation s15WW95HR has considerably smaller seed perturbations, hence prompt convection is much weaker and a smaller GW signal is emitted with $|h_{\text{max}}| \approx 9 \times 10^{-23}$, $E_{\text{GW}} \approx 6 \times 10^{-12} M_{\odot} c^2$, $f_{\text{peak}} \approx 430$ Hz, and $\Delta f_{50} \approx 250$ Hz.

The above numbers and the GW signals shown in figure 5 demonstrate the general seed-perturbation dependence of prompt convection and of the resulting GW burst signal. However, they constitute only two examples and do not bracket the parameter space of possible immediate-postbounce configurations.

Marek et al. [98] also observed prompt convection in their very recent study focussing on the EOS dependence of neutrino and GW emission in the postbounce phase of a nonrotating $15-M_{\odot}$ model. They compared a model run with a soft variant of the Lattimer-Swesty EOS [140] with a counterpart model run with the rather stiff Wolf EOS [188]. Their models produce GW bursts associated with prompt convection that last $\sim 30-40$ ms and produce maximum amplitudes of $\sim 1-2 \times 10^{-22}$ (at 10 kpc) with most of the emission occurring between ~ 60 and ~ 150 Hz. Furthermore, Marek et al. found that the model employing the stiffer nuclear EOS yields up to a factor of 2 larger maximum amplitudes and somewhat higher frequency emission than its softer-EOS counterpart. In the VULCAN/2D models discussed in the above, the GW emission from prompt postbounce convection occurs primarily at $400-700$ Hz. This discrepancy with Marek et al. is most likely due to different numerical seed perturbations and different locations of the former and of the convectively unstable regions.

For a more complete picture and an understanding of the possible prompt-convection GW signals, it will be necessary to conduct a comprehensive study of the quantitative systematics of prompt convection with variations in the magnitude and position of seed perturbations. Ideally such a study should be carried out with a code that uses a nearly perturbation-free grid and with clearly quantifiable perturbations added to the flow shortly before core bounce.

6.2. PNS convection

Owing to a negative radial lepton gradient, PNSs are unstable to convective overturn in a radial interval from ~ 10 km to ~ 30 km [8, 169, 171]. Convection sets in $\sim 20-50$ ms after bounce and may last for several seconds as the PNS slowly contracts and

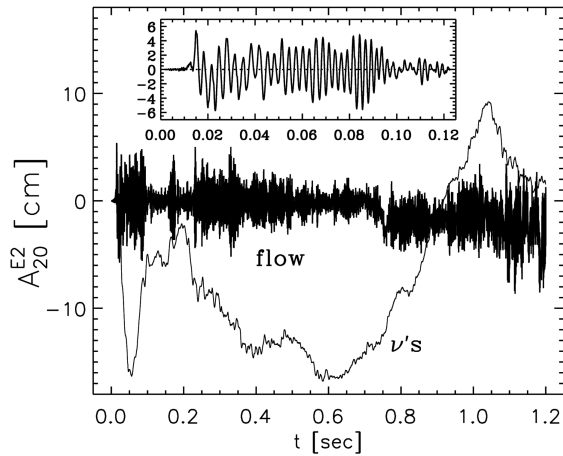


Figure 6. GW signal due to PNS convection in the axisymmetric PNS model of Keil et al. [169, 189] as analyzed by Müller et al. [97] in terms of the quadrupole pure-spin tensor harmonic amplitude A_{20}^{E2} , and $h_+D = \frac{1}{8}\sqrt{\frac{15}{\pi}}\sin^2\theta A_{20}^{E2}$. The matter GW signal and the GW signal due to anisotropic neutrino emission are shown (for a discussion of the latter, see section 8). This figure is figure 5 of [97] and used by kind permission from the authors.

deleptonizes [169] after a successful SN explosion. If the explosion is not successful (or weak) and a black hole is formed, PNS convection and the associated GW emission stop abruptly. Also, if present, large-amplitude PNS core g -modes can distort PNS convection and themselves lead to GW emission much stronger than that due to the convective motions (see section 7.1).

Figure 6 displays the GW signal of PNS convection as analyzed by Müller et al. [97] for the axisymmetric PNS convection simulations of Keil et al. [169, 189] who followed the evolution of an isolated nonrotating PNS core from shortly after core bounce to 1.2 s. Müller et al. reported typical strain amplitudes $|h|$ of $2 - 5 \times 10^{-23}$ (at 10 kpc), an energy emission E_{GW} of $1.6 \times 10^{-10} M_{\odot}c^2$ over 1.2 s and a broad spectrum peaking around ~ 1300 Hz and with most of the energy emitted at 700–1500 Hz.

We analyze the GW signal emitted by PNS convection in the inner ~ 50 km of the aforementioned VULCAN/2D simulations s15WW95 and s15WW95HR in the interval of 20–250 ms after bounce. This interval is chosen, (1) to exclude as much as possible prompt postbounce convection, and, (2), because GWs from PNS core g -modes begin to dominate the convective GW signal at times later than ~ 250 ms in the VULCAN/2D simulations (see section 7.1). For the two calculations, we find comparable GW strain amplitudes $|h|$ in the range of $1 - 4 \times 10^{-23}$ (at 10 kpc). For the high-resolution variant specifically, we find an emitted energy E_{GW} of $\sim 7.0 \times 10^{-12} M_{\odot}c^2$ with a peak of dE_{GW}/df at ~ 350 Hz and most of the energy being emitted within ± 150 Hz about this peak. By scaling E_{GW} to the 1.2 s considered by [97], we obtain $\sim 3.4 \times 10^{-11} M_{\odot}c^2$ which is a factor of ~ 5 smaller than their value. The reason for this discrepancy is most likely the higher average frequency of the GW emission in the model considered by [97]. Note, however, based on the inset plot shown in figure 6 (figure 5 of [97]), one can estimate a dominant emission

frequency around ~ 300 Hz in the first ~ 100 ms of PNS convection. Thus, the higher-frequency emission must take place at later times. This is consistent with the fact that the PNS becomes increasingly compact with time, leading to convection at decreasing radii and generally on smaller spatial scales. As a consequence, one may expect a secular “chirp” of the GW emission frequency from ~ 300 Hz to $\gtrsim 1000$ Hz over ~ 1 s.

6.3. Neutrino-driven Convection and SASI

Neutrino heating below the stalled shock peaks in the inner part of the gain region[‡] and decreases outward (see, e.g., figure 9 of [83]). This establishes a negative radial entropy gradient and makes the gain region unstable to convective overturn (e.g., [8, 124, 168] and references therein). Convection develops within 30–50 ms after bounce in the gain region which extends at these times typically from ~ 50 –80 km out to almost the radius of the stalled shock at ~ 150 –250 km.

The left panel of figure 7 shows the GW signal of neutrino-driven convection and SASI in the VULCAN/2D postbounce calculations s15WW95 and s15WW95HR. The former calculation is carried out to ~ 850 ms after bounce, while the computationally more demanding higher-resolution latter is carried out to ~ 400 ms. In order to exclude PNS convection and PNS g -modes, only regions outside a spherical radius of 60 km are taken into account in computing the GW emission. Since both convection and SASI occur in the same spatial domain and since the SASI-related distortions of the postshock region dynamically modify convection, the GW signals of these two hydrodynamic instabilities cannot be separated cleanly in a SN simulation. Also note that the GW emissions of PNS and neutrino-driven convection/SASI generally interact and in linear theory (and certainly in the Newtonian quadrupole approximation) superpose linearly.

In the calculations considered here, the SASI reaches the non-linear regime around ~ 300 ms and the shock and postshock flow exhibit strong temporally varying distortions at small and large scales (see, e.g., [21]). This is reflected by the GW signal in the form of more rapid time variation and a more pronounced modulation of the late-postbounce emission. For simulation s15WW95, we find maximum GW signal amplitudes around 6×10^{-23} (at 10 kpc; typical amplitudes are about a factor of 2 smaller), $E_{\text{GW}} \approx 7.5 \times 10^{-12} M_{\odot} c^2$ (for the entire 850 ms). The GW emission is rather broadband with most of the energy emitted between 100 and 500 Hz (though with a significant high-frequency tail which is emitted predominantly at postbounce times greater than ~ 400 ms). This is also reflected in the characteristic GW strain spectrum [191],

$$h_{\text{char}}(f) = \frac{1}{D} \sqrt{\frac{2}{\pi^2} \frac{G}{c^3} \frac{dE_{\text{GW}}}{df}}, \quad (2)$$

shown in the right panel of figure 7 and contrasted there with initial and advanced LIGO rms noise levels. Note that h_{char} of the higher-resolution calculation is globally lower due to the shorter period of postbounce time covered by this calculation. Such differences are not limited to simulations: After the onset of explosion, neutrino-driven convection is expected to cease quickly (within 50–100 ms [97]; note that PNS

[‡] The gain region is defined as the region of postbounce space in which neutrino heating dominates over neutrino cooling.

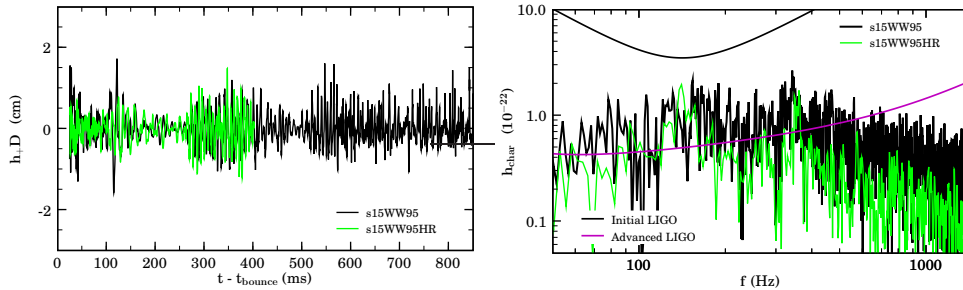


Figure 7. Left: GW signal ($h_+ D$ in units of cm) due to postbounce neutrino-driven convection in the core of a nonrotating $15-M_\odot$ presupernova model of [181]. The first 20 ms of postbounce evolution are cut in order to exclude the initial burst due to prompt convection. The standard-resolution calculation is run to ~ 850 ms after bounce. The development of the SASI to non-linear amplitudes around 300 ms after bounce is reflected in increased amplitudes and more pronounced, higher-frequency variations. In order to study the resolution dependence of the convective GW signal, the high-resolution variant is run to ~ 400 ms after bounce. Because of the stochastic nature of turbulent convection, one cannot expect pointwise convergence of the GW signal, but rather rough agreement in signal amplitudes and characteristic frequencies. The latter is true for s15WW95 and s15WW95HR. The waveforms are available for download from [155]. **Right:** $h_{\text{char}}(f)$ spectra (equation 2) obtained from the s15WW95 and s15WW95HR waveforms for $D = 10$ kpc and compared to initial and burst-mode advanced LIGO h_{rms} noise curves [190]. Note the broadband character of the convective GW emission and the high-frequency tail that is emitted predominantly at late postbounce times and, hence, is particularly pronounced in the standard-resolution variant that is run to ~ 850 ms after bounce. s15WW95HR has overall smaller h_{char} simply because it is run to only ~ 400 ms after bounce.

convection continues). Hence, a real-life SN that explodes at earlier postbounce times will have a smaller integral and frequency-differential E_{GW} (and h_{char}) from neutrino-driven convection/SASI than a counterpart that experiences a later or no explosion at all. The GW signals of s15WW95 and s15WW95HR agree well in average amplitudes and temporal variations in the first ~ 400 ms shown in the left panel of figure 7. For the long-term evolution of a turbulent system one generally cannot expect pointwise convergence for different resolutions. However, agreement “on average” of the GW signals is to be expected.

Müller et al. [97] analyzed the GW emission in 2D simulations of a nonrotating $11.2-M_\odot$ and a slowly rotating $15-M_\odot$ progenitor. They followed the postbounce evolution of their models for 200–250 ms, included an approximate GR potential (see §3), Boltzmann neutrino transport in a ray-by-ray fashion [192], a relatively soft variant of the Lattimer-Swesty EOS [140] and comparable resolution to the aforementioned VULCAN/2D simulations.

The average GW signal amplitudes and time variations found in the VULCAN/2D simulations agree roughly with those of Müller et al. up to ~ 150 ms after bounce, but do not show the large enhancement (by a factor of up to ~ 20 and with rapid time variation around 500–800 Hz) of the GW emission that appear at later times in their simulations. Müller et al. attributed this enhancement to the increased strength of convection, but there may also be a connection to the SASI excursions that become strong around these times in their models. Owing largely to that enhancement, Müller et al. found that most of the GW energy is emitted in the interval of 500–800 Hz

and published total E_{GW} in the range of $10^{-10} - \text{few} \times 10^{-9} M_{\odot} c^2$, roughly two orders of magnitude larger than seen in the VULCAN/2D simulations.

The cause of the discrepancy between the Müller et al. simulations and GW signals and those presented here is most likely related to differences in the employed EOS, the neutrino transport scheme and resulting neutrino luminosities and heating efficiencies, stalled shock radii, and in the development of neutrino-driven convection and the SASI. Furthermore, the enhancement of the GW signal may in part be due to PNS convection or PNS pulsations, since they did not exclude the entire PNS in their analysis.

Kotake et al. [85] focussed on the SASI and employed a simplified approach for modeling postshock flow and neutrino transport. They assumed constant neutrino luminosities and starting from analytic postbounce configurations with a fixed accretion rate of $1 M_{\odot} s^{-1}$ that appear initially stable or only marginally unstable to convection, they studied the dependence of the SASI and SASI/convective GW emission on the assumed neutrino luminosity. The results of Kotake et al. confirm the expectation that higher neutrino luminosities lead to a more pronounced SASI, more SASI-induced turbulence in the postshock region, and greater GW signal amplitudes and emitted energies. For the lowest luminosities considered ($L_{\nu} = 55 \text{ B s}^{-1}$ each for ν_e and $\bar{\nu}_e$), they found maximum amplitudes of $\sim 2.5 \times 10^{-22}$ and maximum h_{char} of $\sim 10^{-21}$ (dependent, of course, on the duration of the simulation) at f_{peak} of 100–200 Hz. The sum of the time-dependent ν_e and $\bar{\nu}_e$ luminosities in the s15WW95 postbounce simulations with VULCAN/2D varies from 85 B s^{-1} at ~ 100 ms to 50 B s^{-1} at $\gtrsim 400$ ms after bounce. It is at all postbounce times smaller than the 110 B s^{-1} assumed by Kotake et al. Considering the dependence of the SASI and convective dynamics on the neutrino luminosity, it is not surprising that Kotake et al. found significantly stronger GW emission than the analysis of the VULCAN/2D simulations suggests.

Marek et al. [98] extended the previously discussed work of Müller et al. [97] and considered for a nonrotating $15-M_{\odot}$ model variations of the convective/SASI dynamics and the associated GW emission with the stiffness of the nuclear EOS. They followed their calculations to 400 ms after bounce and analyzed in detail the GW signal due to matter dynamics and anisotropic neutrino radiation fields (for a summary of the latter, see section 8.2). The qualitative features of the matter GW signals their models are qualitatively fairly similar to those obtained with VULCAN/2D (shown in figure 7). Marek et al. found that the GW signal amplitudes and typical emission frequencies increase with postbounce time and with the growing strength of the SASI-driven shock distortions. Their models produce peak amplitudes around 5×10^{-22} (at 10 kpc) and average amplitudes about a factor of 2 smaller. Furthermore, Marek et al. reported that the SASI-moderated aspherical convective motions in the low-density postshock gain layer lead to GW emission at frequencies up to ~ 200 Hz. Those GWs, however, make up only the subdominant, low-frequency part of the total emission, which in their models is dominated by the GWs emitted from deeper, higher-density regions where aspherical accretion downstreams are decelerated and perturb the PNS core.

Comparing a model run with a soft variant of the Lattimer-Swesty EOS [140] with a counterpart model run with the stiff Wolff EOS [188], Marek et al. found that the Lattimer-Swesty EOS model yields higher-amplitude (by up to a factor of 2), higher-frequency (spectral peak at 600 – 800 Hz vs. 300 – 600 Hz) GW emission. These differences are a consequence of the more compact PNS and resulting harder neutrino

Table 2. Semi-quantitative summary of the GW emission by aspherical fluid motions associated with convection and SASI. The numbers for prompt convection are based on VULCAN/2D simulations presented here and in [23] and on simulations carried out by Marek et al. [98]. The GW emission characteristics of PNS convection and neutrino-driven convection/SASI are based on the results of [23, 97, 98] and the VULCAN/2D simulations presented in this article. We provide estimates for the typical GW strain at 10 kpc, the typical emission frequency f , the duration of the emission Δt , and the emitted energy E_{GW} in GWs. In addition, we list processes and factors that may limit the duration of the GW emission. All numbers, including various upper and lower limits, should be regarded as estimates that require confirmation by future studies and that, at best, may guide expectations.

Process	Typical $ h $ (at 10 kpc)	Typical f (Hz)	Duration Δt (ms)	E_{GW} ($10^{-10} M_{\odot} c^2$)	Limiting Factors or Processes
Prompt Convection	$10^{-23} - 10^{-21}$ (Emission characteristics depend on seed perturbations.)	50 – 1000	0 – \sim 30	$\lesssim 0.01 - 10$	Seed perturbations, entropy/lepton gradient, rotation
PNS Convection	$2 - 5 \times 10^{-23}$	300 – 1500	500 – several 1000	$\lesssim 1.3(\frac{\Delta t}{1s})$	rotation, BH formation, strong PNS g -modes
Neutrino- driven Convection and SASI	$10^{-23} - 10^{-22}$ (peaks up to 10^{-21})	100 – 800	100 – \gtrsim 1000	$\gtrsim 0.01(\frac{\Delta t}{100ms})$ $\lesssim 15(\frac{\Delta t}{100ms})$	rotation, explosion, BH formation

spectra and increased neutrino luminosities which, in turn, result in increased neutrino heating and more vigorous convection/SASI. This quantitative result is of particular importance, since it demonstrates that – despite the stochastic, untemplateable nature of the convective/SASI GW signal – key microphysical aspects can still be constrained via the observation of GWs emitted by convection/SASI.

To conclude this section, we point out that in consideration of the still small set of mostly axisymmetric studies that have addressed GW emission from neutrino-driven convection/SASI, the currently available GW signal estimates should be regarded only as examples that may guide expectations. They are not yet robust and many more simulations will be needed to systematically (qualitatively and quantitatively) study the range of possible postbounce evolutions and corresponding incarnations of convective overturn. In particular, it will be important to quantify the dependence on progenitor structure and explore the dynamics of convection and SASI in 3D.

Table 2 provides an overview of the GW emission from prompt, PNS, and neutrino-driven convection / SASI. We provide rough values for typical $|h|$, typical emission frequencies, emission durations, emitted energies, and list factors and processes that may inhibit the development or shorten the duration of the individual emission processes.

7. Non-radial PNS Pulsations

PNSs and cold NSs can pulsate in a multitude of ways (e.g., [61, 146]) and their non-radial pulsation modes of quadrupole and higher order emit GWs. Polar (even-parity) fluid modes are grouped into the lower-frequency g -modes (buoyancy modes, restoring force gravity, require compositional or thermal gradients) and the higher-

frequency p -modes (restoring force pressure), separated in frequency by the f -mode (fundamental mode without nodes inside the star). Axial (odd-parity) fluid modes are modes whose restoring force is the Coriolis force, hence they require rotation and are degenerate at zero frequency in the nonrotating limit. Modes of mixed axial and polar character, so-called hybrid modes, exist as well (e.g., [146, 193]). r -modes (Rossby waves), a particular group of axial inertial modes, are strongly unstable to the GW-back-reaction Chandrasekhar-Friedman-Schutz (CFS) instability [194, 195] at all rotation rates [61, 196]. In PNSs, r -modes have growth times of the order of seconds [197] and appear to saturate at low amplitudes [198]. Hence, they are unlikely to be relevant sources of GWs in the first second of a PNS's life.

In addition to fluid modes there exist polar and axial modes of spacetime curvature, low-frequency s -modes and high-frequency w -modes, that are weakly coupled to matter (e.g., [60, 146] and references therein).

Studies of non-radial pulsations of cold NSs as emission processes of GWs have a long history (see, e.g., [60, 61, 199, 200] and references therein). In the core-collapse SN context, non-radial PNS oscillation modes and damping by GW emission and other processes were first considered by McDermott et al. [201, 202], Finn [203], and Reisenegger and Goldreich [204].

Recently, in a series of papers, Ferrari and collaborators [205, 206, 207, 208] studied in GR perturbation theory the PNS non-radial mode spectrum and the GW emission from PNS pulsations on the basis of detailed spherically-symmetric PNS cooling models. They considered mode amplification by the CFS instability in rotating PNSs, but did not study the excitation of non-radial modes in the nonrotating limit. Assuming the presence of pulsational energy, they provided estimates in [205] for the typical $|h|$ and E_{GW} necessary for a particular mode to be detectable by current and future GW observatories. According to their estimates for a nonrotating or very slowly rotating PNS, the most efficiently radiating mode, the lowest-order quadrupole g -mode (frequency $f \approx 500 - 600$ Hz), would need to emit GWs at a typical $|h|$ of $\sim 8 \times 10^{-22}$ (at 10 kpc) and emit a total E_{GW} of $\sim 4 \times 10^{-8} M_{\odot} c^2$ to be detectable by initial-LIGO-class detectors at a distance of 10 kpc. In the case of more rapid rotation, the g -mode frequencies are lower and closer to the maximum detector sensitivity, leading to lower required $|h|$ and E_{GW} .

Passamonti et al. [209, 210] explored the excitation of higher-order non-radial polar modes by non-linear couplings of radial and non-radial eigenmodes that are excited in the early postbounce ring-down phase of any core-collapse event[§]. Such couplings were first suggested by Eardley [47]. Passamonti et al. employed a GR perturbative framework and approximated the PNS by a simple polytropic stellar structure (which excludes g -modes). Their results indicate that the radial and non-radial fundamental oscillation modes present in the very early postbounce phase will couple and give rise to a rich spectrum of daughter modes^{||}. The strongest of these non-linear modes could be detectable by advanced LIGO-class detectors from a galactic event and their spectral information would provide additional insight into the high-density nuclear EOS and the internal structure of a newborn PNS.

The pulsational mode structure of rapidly rotating NS/PNSs cannot be

[§] In a related work, Passamonti et al. [211] also studied the coupling of radial modes with non-radial axial modes.

^{||} Such radial–non-radial mode couplings have recently been observed also in numerical models of phase-transition-induced collapse of NSs [212].

determined reliably by perturbative methods and GR hydrodynamic simulations must be carried out to obtain the spatial and spectral mode characteristics. Dimmelmeier et al. [199] recently carried out the first extensive study of the axisymmetric mode structure of rapidly rotating polytropic NS models in CFC GR [100], going beyond the Cowling approximation employed by most previous studies (e.g., [213] and references therein). The mode structure of rapidly rotating finite-temperature PNSs remains to be studied.

7.1. Protoneutron Star g -Mode Pulsations in the Context of the Acoustic Mechanism for Core-Collapse Supernova Explosions

Burrows et al. [21, 22], in their simulations that lead to the proposition of the *acoustic mechanism* for core-collapse SN explosions, have discovered the excitation of PNS core g -modes by turbulence and by accretion downstreams through the unstable and highly-deformed stalled shock that experiences the SASI. The pulsations damp by the emission of strong sound waves and do not ebb until accretion subsides. As discussed in [21, 22], these PNS core g -mode pulsations reach nonlinear amplitudes and act as transducers for the conversion of accretion gravitational energy into acoustic power that is deposited in the postshock region and may be sufficient to drive an explosion. Although promising, this acoustic SN mechanism remains controversial (see, e.g., [9, 24, 25]) and has yet to be confirmed by other groups. In particular, Weinberg et al. [25] pointed out that the saturation amplitude of the PNS g -modes may be limited by non-linear model coupling via a parametric instability that cannot be resolved in present simulations. In addition, there are indications [17, 83] that rapid rotation significantly weakens convection and modifies the SASI and thus may weaken the driving mechanism for the PNS core g -modes.

Burrows et al. found that the fundamental $\ell = 1$ g -mode of the PNS core is most easily and first excited in their models. Higher-order eigenmodes and, through non-linear couplings, harmonics of eigenmodes and other modes with complicated spatial structures appear at later times. Ott et al. [23] analyzed the GW emission from the quadrupole components of the PNS core pulsations in the original nonrotating $11-M_{\odot}$ model presented in [21] and, in addition, for a slowly-rotating $15-M_{\odot}$ model and a nonrotating rather extreme $25-M_{\odot}$ model with a very extended and massive iron core. For these models they found maximum GW amplitudes $|h_{\max}|$ of $\sim 1.3 \times 10^{-21}$ (at 10 kpc) for their $11-M_{\odot}$ and $15-M_{\odot}$ models and $\sim 5 \times 10^{-20}$ (at 10 kpc) for the $25-M_{\odot}$ model. The total emitted E_{GW} s were around $1.5 \times 10^{-8} M_{\odot} c^2$ in the $11-M_{\odot}$ and $15-M_{\odot}$ model, while the $25-M_{\odot}$ model emitted an amazing $8 \times 10^{-5} M_{\odot} c^2$. GW back-reaction effects, though neglected in [23], are probably relevant for this latter model [42]. Most of the emission in these models took place in frequency space at $\sim 650 \pm 100$ Hz and $\sim 900 \pm 100$ Hz.

In [22], Burrows et al. considered an extended set of nonrotating progenitors, covering the mass range from $11.2 M_{\odot}$ to $25.0 M_{\odot}$ solar masses, and using presupernova models of [137, 214]‡. In the following, we present their previously unpublished GW signals and summarize the key signal characteristics in table 3. The waveforms and E_{GW} spectra of all models can be obtained from [155].

The left panel of figure 8 depicts the GW signal obtained from models s15.0

‡ Note that the precollapse models used in [21, 23] were taken from [181] and [142]. Model s25.0 of [22] should not be confused with model s25WW of [23].

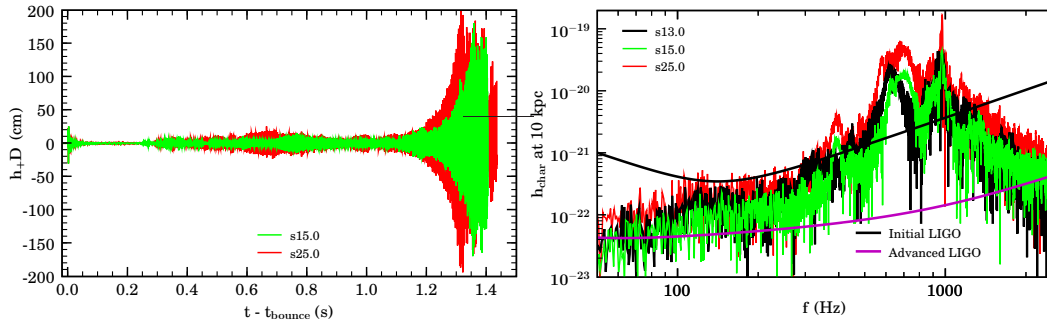


Figure 8. GW emission in a set of representative models from [22]. **Left:** GW wave signal (h_+D in units of cm) as a function of postbounce time in the nonrotating models s25.0 (red) and s15.0 (green). The burst shortly after core bounce is due to prompt convection (see section 6). Around 300–400 ms, the GW emission becomes dominated by the growing g -mode amplitudes, but stays at relatively small amplitudes initially. The core pulsations become more vigorous at later times, leading to the emission of large-amplitude GWs. Explosion sets in around ~ 1.0 – 1.4 s after bounce and in some cases is unipolar (see [21, 22]) – the star explodes on one side while accretion continues on the other. All waveforms are available from [155]. **Right:** Characteristic GW strain spectra (equation 2 and [191]) of various models of [22] contrasted with the initial and advanced LIGO rms noise curves [190] for a source distance of 10 kpc. Note that the spectra of all models exhibit a narrow primary peak near 950 Hz and a broader secondary peak around 600–700 Hz.

($15 M_\odot$) and s25.0 ($25 M_\odot$) as a function of postbounce time. There is little variation in the qualitative features of the GW signal throughout the model set considered by [22]. Hence, models s15.0 and s25.0 are quite representative picks. Core bounce in these models is marked by a GW burst that is due to prompt convective overturn setting in very shortly after bounce (see section 6.1). Typical peak GW amplitudes are around $\sim 1 \times 10^{-21}$ at 10 kpc and most of the energy is emitted in a frequency interval of 500–800 Hz. The prompt convection subsides quickly, and during the interval from ~ 20 ms to ~ 300 ms the GW signal is dominated by convection in the PNS and in the postshock region. The PNS core pulsations reach significant amplitudes at 300–400 ms after bounce and the GW emission from their quadrupole components starts to dominate the overall GW signal. From ~ 300 ms to ~ 1.1 s the models emit quasi-continuous GWs with maximum amplitudes in the range of $\sim 3 \times 10^{-22}$ – 8×10^{-22} at 10 kpc, modulated on a timescale of ~ 100 ms by variations in the SASI and accretion-dependent excitation (and damping) of the core pulsations. At postbounce times greater than ~ 1.1 s, the quadrupole components of the core pulsations reach very large amplitudes (possibly through the excitation of an $\ell = 2$ eigenmode [23]), leading to a significant increase in the GW amplitudes up to $\sim 7 \times 10^{-21}$ ($\sim 4 \times 10^{-21}$) at 10 kpc in model s25.0 (s15.0). The other models studied by Burrows et al. [22] reach comparable $|h_{\text{max}}|$ (see table 3).

All models of Burrows et al. [22] explode between ~ 1.0 s and 1.4 s after bounce and the simulations were stopped when the shock reached the outer boundary of the computational grid. In models that exploded globally, the PNS core pulsations and the corresponding GW signal generally subsided after the onset of explosion. However, in a few models, the explosion was unipolar, setting in along one of the poles while accretion continued on the opposite side, sustaining to some extent the core pulsations

Table 3. GW data summary for models calculated by Burrows et al. [22] whose GW signals have not previously been published. In addition, the GW emission characteristics of the models of [21, 23] are listed for completeness. Δt is the amount of postbounce time covered in each model, $|h_{+, \max}|$ is the overall maximum GW amplitude scaled to 10 kpc distance, $h_{\text{char}, \max}$ is the global maximum of the characteristic strain spectrum [191], f_{peak} is the frequency of the global maximum and δf is the FWHM. Data for the secondary pronounced peak in $h_{\text{char}}(f)$ are given and all related quantities have the subscript 2. E_{GW} is the total energy radiated in GWs. Note that the values given for $|h_{\max}|$ in [23] are slightly different from those presented here for models of [23]. This is due to a small error in the analysis routines used by [23]. Also note that model s25WW of [23] uses a rather extreme 25- M_{\odot} precollapse model of [181] with a very extended and massive iron core and a very shallow density gradient.

Model	Δt (ms)	$ h_{+, \max} $ (10^{-21} at 10 kpc)	Primary h_{char} peak			Secondary h_{char} peak			E_{GW} (10^{-7} $M_{\odot} c^2$)
			$h_{\text{char}, \max}$ (10^{-21} at 10 kpc)	f_{peak} (Hz)	δf (Hz)	$h_{\text{char}, \max 2}$ (10^{-21} at 10 kpc)	$f_{\text{peak} 2}$ (Hz)	δf_2 (Hz)	
Models of [22]									
s11.2	1496	1.26	40.3	910	~ 100	5.5	605	~ 100	0.60
s13.0	1447	4.00	44.3	934	~ 75	27.4	613	~ 90	1.03
s15.0	1404	3.75	45.8	970	~ 35	22.0	690	~ 130	4.30
s20.0	1715	3.61	61.6	992	~ 20	33.4	630	~ 200	2.36
s25.0	1434	6.93	70.9	969	~ 10	64.7	672	~ 200	7.25
nomoto13	1237	0.77	22.1	907	~ 40	41.8	602	~ 80	0.12
nomoto15	1725	1.04	43.7	997	~ 100	44.5	604	~ 100	0.70
Models of [23]									
s11WW	1045	1.58	22.8	654	~ 50	8.5	895	~ 40	0.16
m15b6	927	0.98	19.3	660	~ 20	7.9	822	~ 30	0.14
s25WW	1110	49.91	2514.3	937	~ 10	707.2	790	~ 20	824.28

and prolonging the GW emission.

In the right panel of figure 8, characteristic strain spectra $h_{\text{char}}(f)$ (equation 2; for a source distance of 10 kpc) are shown for models s13.0, s15.0, and s25.0. More massive progenitors generally tend to have higher accretion rates \S , tend to explode later, reach higher $|h_{\max}|$, have higher total E_{GW} , and more narrow peaks in dE_{GW}/df (see table 3). As a consequence, the maximum values of h_{char} generally increase with progenitor mass.

It is interesting to note that h_{char} exhibits two pronounced peaks in all considered models. The primary, quite narrow peak is centered in frequency around 900–1000 Hz while the secondary, smaller and broader peak is located in the frequency range 500–700 Hz. This is due to the complicated time-dependent mode structure present in the pulsating PNS core and is also highlighted by figure 9 which provides a frequency-time analysis of the GW energy spectrum dE_{GW}/df of model s15.0. Due to changes in the hydrodynamic and thermodynamic structure of the PNS, the g -mode frequencies vary (as do the frequencies of other mode families) with time [205]. In addition, higher-order harmonics and modes with complicated spatial structure are excited and their quadrupole parts emit GWs. At early to intermediate postbounce times, the emission

\S Note that the presupernova models of [137] behave non-monotonically in the scaling of (iron) core mass and density profile in the mass range from ~ 15 to $\sim 20 M_{\odot}$. See also [22, 108].

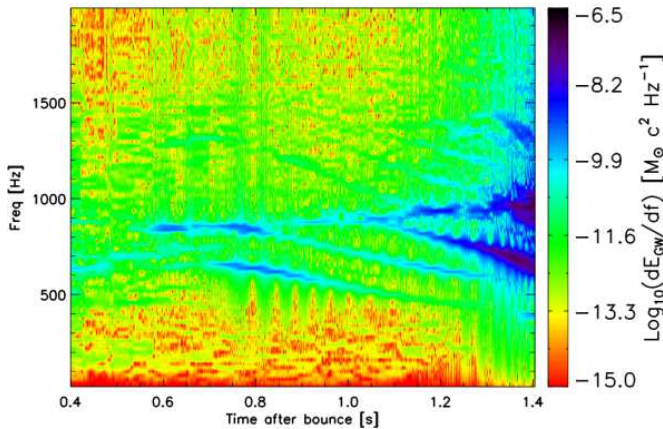


Figure 9. Frequency-time evolution of the GW energy spectrum dE_{GW}/df in model s15.0 of [22], computed with a 50 ms sampling interval and a step width of 1 ms. Shown is the interval from 0.4 s after core bounce to the end of the simulation. Given the complex thermodynamic structure of a hot PNS, the mode spectrum reflected in dE_{GW}/df is rather complicated and exhibits significant temporal variations in mode frequencies and preferred modes. Note that the two strong emission regions around 900–1000 Hz and 600–800 Hz correspond to the the primary and secondary peak in $h_{\text{char}}(f)$ shown in the right panel of figure 8.

occurs mainly from quadrupole components with frequencies around ~ 600 Hz and ~ 850 Hz. The frequencies initially show a weak upward trend, but decrease beginning at around ~ 700 ms. At late times, most of the energy is being emitted around ~ 850 Hz and ~ 600 Hz–700 Hz, but this time by quadrupole components of modes who have descended from higher frequencies.

The PNS core g -mode pulsations may arguably be so far the strongest proposed emission process for GWs in core-collapse SNe. Observing GWs due to PNS g -modes and capturing the time-evolution of the GW spectrum would provide us with invaluable information that could be used, via comparison with model calculations, to reconstruct the hydrodynamic and thermodynamic structure and evolution of a very young PNS. In addition, and since the acoustic mechanism for SN explosions and the strong PNS core g -modes are almost invariably linked, the observation or the non-observation of the g -mode GW signal from a nearby core-collapse SN may be used to test the acoustic SN mechanism (see also section 11).

Nevertheless, it is important to keep in mind that the viability of the acoustic SN mechanism is still unclear and that the dependence on dimensionality (2D vs. 3D), rotation, equation of state, description of gravity (Newtonian vs. GR) and the possibility of mode saturation at low amplitudes [25] remain to be explored in detail.

8. Anisotropic Neutrino Emission

Not only aspherical fluid motion, but in more general terms, any accelerated transport of energy with a non-zero quadrupole and/or higher-order component emits GWs. For the case of anisotropic radiation of neutrinos from a distant point source, this has been first realized in linear theory via the direct solution of the inhomogeneous

wave equation by Epstein [81] (but, see also Turner’s independent derivation in the zero-frequency limit [82]).

Burrows & Hayes [123] and Müller & Janka [124] were the first authors to implement the formalism. It has since been employed in a number of other studies [23, 35, 85, 97, 98, 179, 215]. In the following, we present a short overview on the formalism as used by [123, 124] in axisymmetry. More details and the generalization to 3D can be found in [35, 124].

For axial symmetry, [123, 124] write the dimensionless GW strain for an observer positioned in the equatorial plane as

$$h_{+,eq}^{TT}(t) = \frac{2G}{c^4 D} \int_{-\infty}^{t-D/c} \alpha(t') L_\nu(t') dt' , \quad (3)$$

where $L_\nu(t)$ is the total neutrino luminosity and $\alpha(t)$ is the instantaneous neutrino radiation anisotropy that includes the transverse-traceless projections [124]. It is defined as

$$\alpha(t) = \frac{1}{L_\nu(t)} \int_{4\pi} \Psi(\vartheta', \varphi') \frac{dL_\nu(\vec{\Omega}', t)}{d\Omega'} d\Omega' , \quad (4)$$

where $dL_\nu(\vec{\Omega}, t)/d\Omega$ is the energy radiated at time t per unit of time and per unit of solid angle into direction $\vec{\Omega}$ with

$$L_\nu(t) = \int_{4\pi} \frac{dL_\nu(\vec{\Omega}', t)}{d\Omega'} d\Omega' . \quad (5)$$

$\Psi(\vartheta, \varphi)$ represents the angle dependent factors in terms of source coordinate system angles ϑ and φ and depends on the particular GW polarization and the observer position relative to the source. In axisymmetry, $h_{\times}^{TT} = 0$ everywhere, and $h_{+}^{TT} = 0$ along the axis of symmetry. For an observer located in the equatorial plane, observing the + GW polarization, $\Psi(\vartheta, \varphi)$ is given [35, 124] by

$$\Psi(\vartheta, \varphi) = (1 + \sin \vartheta \cos \varphi) \frac{\cos^2 \vartheta - \sin^2 \vartheta \sin^2 \varphi}{\cos^2 \vartheta + \sin^2 \vartheta \sin^2 \varphi} . \quad (6)$$

In axisymmetry, there is no φ dependence of the luminosity. By integrating $\Psi(\vartheta, \varphi)$ over φ , equations 4 and 6 combine to [35, 85],

$$\alpha(t) = \frac{2\pi}{L_\nu(t)} \int_0^\pi \sin \theta' (-1 + 2|\cos \theta'|) \frac{dL_\nu(\theta', t)}{d\theta'} d\theta' . \quad (7)$$

Note that the GW signal due to neutrinos observed at time $t + D/c$ contains contributions from anisotropies in the neutrino radiation field at all times prior t . This leads to a memory effect in the GW signal, leaving behind a constant (“DC”) offset after the anisotropic neutrino emission subsides. Largely-aspherical mass ejection can lead to a similar GW memory (see section 9). The implications and detectability of such GW bursts with memory were discussed in [34, 216].

In the context of massive star collapse and core-collapse SNe, anisotropic neutrino radiation and the associated emission of GWs may arise (a) from rotationally-deformed PNSs [35, 42, 97, 215], (b) from convective overturn and SASI [23, 42, 85, 97, 98, 124], and (c) from global asymmetries in the (precollapse) matter distribution [123, 179].

The extraction of GWs due to neutrino radiation field anisotropies requires that the underlying simulation was carried out with some form of neutrino transport.

Unfortunately, the set of presently employed approaches to neutrino transport generally yield different results for the degree of anisotropy of the neutrino radiation field for the same hydrodynamic configuration. For example, any ray-by-ray scheme (Boltzmann transport or MGFLD) that implements 2D neutrino transport via many solutions of 1D transport problems along radial rays, even if neighboring rays are coupled, tends to overestimate local and global anisotropies. On the other hand, a full-2D MGFLD approach tends to smooth out anisotropies in the radiation field, in particular at low optical depths. Ideally, neutrino transport should be carried out in 2D (or 3D) with energy and momentum-space angle-dependence. Ott et al. [83] have recently carried out such simulations using the S_n method (e.g., [217]), but due to limited number of momentum-space angles that could be used in long-term evolutions, anisotropies in the neutrino radiation field are dominated by poor numerical resolution.

When interpreting any results on the GW signal emitted by anisotropic neutrino radiation obtained with current codes, the dependence on the neutrino transport formulation and numerics should be kept in mind.

8.1. Rapid Rotation

Because of the action of centrifugal forces, a rapidly-rotating PNS has an oblate shape. The neutrino radiation field and its energy-dependent neutrinospheres follow the matter distribution. Because of the more compact polar and more extended equatorial density distribution, neutrinos decouple from matter at smaller radii along the poles than on the equator. Depending on the degree of rotational deformation, this can lead to very large pole-equator asymmetries in the neutrino radiation fields, resulting in the emission of GWs (see, e.g., [83, 215, 218, 219]). Since the qualitative shape of the asymmetry does not vary with time (viz. the PNS stays oblate), the GW signal is monotonically growing in amplitude and exhibits slow time variation.

Dessart et al. [215] and Ott [42] analyzed the GW emission due to aspherical mass motions and asymmetric neutrino radiation fields in the axisymmetric Newtonian accretion-induced collapse (AIC) simulations of Dessart et al. [215]. An AIC event in a massive ONeMg white dwarf is expected to leave behind a PNS that is similar in many ways to a PNS formed in standard iron core collapse. The two AIC models considered by Dessart et al. [215] yielded rapidly rotating PNSs with postbounce β s of ~ 0.05 and ~ 0.25 for their $1.46-M_\odot$ model and $1.92-M_\odot$ model, respectively. Dessart et al. employed a 2D MGFLD approach to neutrino transport and, hence, the numbers given below for the GW emission due to neutrinos may be underestimating the true signal strength.

Figure 10 shows the contribution of anisotropic neutrino emission to the GW signal in the AIC models. At bounce, the signal shows the greatest variation due to the strong electron-neutrino burst. After bounce, the amplitude slowly but continuously rises. At the end of the simulations, $|h_{\max}|$ at 10 kpc is $\sim 3.6 \times 10^{-21}$ ($\sim 0.55 \times 10^{-21}$) in the $1.92-M_\odot$ ($1.46-M_\odot$) model. The amplitude continues to grow in the subsequent cooling phase, but its growth rate decreases continuously, since the neutrino luminosity L_ν is dropping at a greater rate than the anisotropy parameter α is increasing. In the frequency domain, the GW emission due to neutrinos occurs at low frequencies and dE_{GW}/df peaks in the range of 0–10 Hz. The total emitted E_{GW} is $\sim 2 \times 10^{-11} M_\odot c^2$ ($\sim 1 \times 10^{-12} M_\odot c^2$) in the $1.92-M_\odot$ ($1.46-M_\odot$) model||.

|| Note that the numbers for E_{GW} given here differ from those stated in [215]. This is due to an

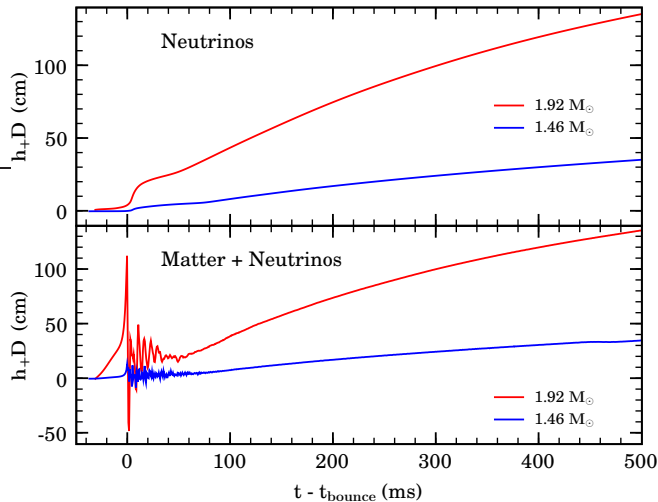


Figure 10. GW signal from the rapidly-rotating accretion-induced collapse (AIC) simulations of Dessart et al. [215] as analyzed in [42]. The $1.92-M_{\odot}$ model has a postbounce β of ~ 0.25 while the $1.46-M_{\odot}$ model is rotating much more slowly with postbounce $\beta \lesssim 0.05$. **Top:** GW signal (h_+D in units of cm) emitted by anisotropic neutrino radiation. The time is given with respect to the time of bounce and the first 500 ms after bounce are shown. Note the very slow time variation of the signal which is due to the time integral in equation 3 and to the slowly varying anisotropy of the radiation field owing to the secular contraction of the PNS. The GW signal due to neutrinos was extracted at a spherical radius of 300 km (200 km) in the $1.92-M_{\odot}$ ($1.46-M_{\odot}$) model. **Bottom:** Combined matter and neutrino GW signal. The GW signal data are available for download from [155].

Kotake et al. [35] showed example results of their unpublished work on the GW signal from rapidly-rotating iron core collapse. Unfortunately, they provided only the GW signal from core bounce and did not provide overall signal characteristics that could be compared with the AIC models of Dessart et al.

Müller et al. [97] studied the GW emission due to neutrinos in a relatively slowly rotating $15-M_{\odot}$ model. They found an almost monotonically-growing GW signal qualitatively similar to those shown in figure 10 with a maximum amplitude at 10 kpc of $\sim 1.3 \times 10^{-21}$ at the end of their simulation (~ 270 ms after bounce). Since their $15-M_{\odot}$ model, in contrast to the AIC models of Dessart et al., exhibited significant convective overturn, its GW signal contains higher-frequency ($\sim 20 - 100$ Hz) components that are due to either locally-enhanced neutrino emission from rapid downflows or variations in neutrino absorption due to convective overturn.

Given the above listed results, the GW signal due to anisotropic neutrino emission associated with rapid PNS rotation is emitted at too low frequencies and is not sufficiently energetic to be a good candidate for detection by current and planned ground-based GW observatories even if the stellar collapse event occurs within the Milky Way. The situation may be different in the case of moderate rotation studied by Müller et al. [97] in which the GW signal contains higher-frequency contributions error in the GW analysis of [215].

from convection/down-stream-induced neutrino radiation anisotropies. According to the results of Müller et al., the neutrino GW signal of such cores may be detectable with advanced LIGO-class detectors for a galactic source.

8.2. Convection and SASI

Convection and SASI introduce asphericity into the postshock flow, leading, among other things, (1) to spatially varying neutrino cooling/heating in the region between shock and PNS core and (2) to accretion funnels that allow for rapid downflow of material and locally enhanced neutrino emission where an accretion funnel hits the PNS core. Janka & Müller [124] first investigated (though with simplified neutrino transport and an artificial inner core boundary) the GW emission from anisotropic neutrino radiation fields owing to postbounce convection and accretion downstreams. Since they provided only GW signals for which neutrino and baryonic matter contributions were summed up, it is difficult to extract the neutrino component. A rough estimate gives modest peak amplitudes in the range of 5×10^{-24} to $\lesssim 1 \times 10^{-22}$ at 10 kpc and the typical slow waveform variation.

More recently, Müller et al. [97], using a ray-by-ray Boltzmann neutrino-transport scheme and a gravitational potential whose monopole term is general relativistic, investigated the emission of GWs due to neutrinos in the first $\sim 200 - 270$ ms after bounce in a slowly-rotating $15-M_{\odot}$ model (discussed above in section 8.1) and a non-rotating $11-M_{\odot}$ model. In the latter, the GW signal due anisotropic neutrino emission reflects the stochastic nature of postbounce convection and varies slowly (typical frequencies around $10 - 20$ Hz) with no clear long-term trend, reaching maximum amplitudes of $\sim 1.4 \times 10^{-22}$ at 10 kpc. Due to the low-frequency variation, the emitted E_{GW} can be expected to be small, was not stated explicitly by the authors, and is likely to be in or below the ball park of the numbers mentioned in section 8.1 for rapidly-rotating AIC models. In contrast to their slowly-rotating $15-M_{\odot}$ model, the neutrino GW signal of the non-rotating $11-M_{\odot}$ model is unlikely to be detectable even by advanced LIGO-class observatories and when occurring at 10 kpc distance.

In addition to the $15-M_{\odot}$ and $11-M_{\odot}$ models, Müller et al. also considered the GWs emitted by anisotropic neutrino radiation in a PNS convection model of Keil et al. [169, 189] (see section 6.2 and figure 6). The GW signal is qualitatively and quantitatively similar to what Müller et al. observed in their full $11-M_{\odot}$ progenitor. However, before explosion, the true asymptotic neutrino anisotropy must be extracted outside the optically-semi-transparent postshock layer (see, e.g., [98]) which was not included in the PNS model of Keil et al. At post-explosion times, the neutrinos practically free-stream from the PNS surface and the GW signal from the PNS simulation becomes more relevant.

Using 2D-MGFLD, Ott et al. [23, 42, 155] found for three long-term postbounce models in the mass range from 11 to $25 M_{\odot}$ maximum amplitudes $|h_{\text{max}}|$ of $\sim 1.3 \times 10^{-23}$ to $\sim 5.5 \times 10^{-23}$ (at 10 kpc) built up over the ~ 1 s of postbounce time covered by the simulations and extracted at a radius of 200 km. The neutrino GW signals in these models exhibit a systematic trend to negative, in absolute value continuously growing amplitudes. The total emitted E_{GW} due to neutrinos were small, below $\sim 1 \times 10^{-13} M_{\odot}c^2$ and most of the energy emission took place at frequencies below ~ 10 Hz. Since MGFLD has the tendency to smooth out radiation-field anisotropies [83], the above numbers unfortunately depend on the extraction

radius and should be regarded as underestimates.

Kotake et al. [85], using a simplified approach to neutrino heating and cooling, studied the GW emission from angular variations in the neutrino cooling in their models that were focussed on the non-linear development of the SASI. They found quasi-monotonically growing GW signals that showed slow variations (1–50 Hz) and reached maximum values after ~ 500 ms of $2.0\text{--}3.5 \times 10^{-20}$ (at 10 kpc). The GW signal amplitudes found by Kotake et al. are systematically positive which the authors attributed to SASI-enhanced polar neutrino emission. The emitted E_{GW} were in the range of $2 - 6 \times 10^{-10} M_{\odot}c^2$. These large numbers are a most likely a consequence of the neutrino luminosities they imposed which were a factor of 5 to 10 larger than in more realistic simulations [23, 97] and lead to very vigorous overturn and SASI.

Marek et al. [98] studied the GW emission from anisotropic neutrino radiation fields in a nonrotating $15\text{-}M_{\odot}$ model that was run with two nuclear EOS of different stiffness (see also the discussion of their study in section 6.3). Similarly to Ott et al. [23, 42], but in disagreement with the less detailed study of Kotake et al. [85], they found a continuously (in absolute value) growing negative GW signal. According to their detailed analysis, this negative signal is a consequence of enhanced equatorial neutrino emission in the postshock region. At 400 ms after bounce, their Lattimer-Swesty EOS [140] model reaches $|h|$ of $\sim 1.2 \times 10^{-21}$ (at 10 kpc) while the model run with the stiffer Wolff EOS [188] exhibits a smaller $|h|$ of $\sim 5.7 \times 10^{-22}$. These $|h|$ are larger than the typical amplitudes of GWs emitted by the matter dynamics associated with convection/SASI (section 6.3). However, in agreement with previous studies, Marek et al. [98] provided GW spectra indicating emission predominantly at frequencies $\lesssim 20$ Hz, making the component of the overall GW signal associated with anisotropic neutrino emission very difficult to detect for ground-based detectors whose sensitivity is limited by gravity-gradient and seismic noise at low frequencies (e.g., [33]).

8.3. Global Asymmetries

Large-scale density perturbations that may be due to inhomogeneities in the iron core, silicon, and/or oxygen shells lead to globally asymmetric postbounce mass motions resulting in large angular variations in the neutrino luminosity (see also section 9.2). The GWs emission due to neutrinos in such a globally asymmetric core-collapse event has first been considered by Burrows and Hayes [123] in 2D, using a ray-by-ray gray flux-limited diffusion approach [167]. Their single model with a 15% precollapse density perturbation near the north pole produced a GW signal with a large $|h_{\text{max}}|$ of $\sim 3.5 \times 10^{-21}$ (at 10 kpc). The signal, shown in the right-hand panel of figure 11, exhibits a strong burst at core bounce (with ~ 500 Hz characteristic frequency) and a subsequent slow growth to the final amplitude (the model was tracked to only ~ 70 ms after bounce). The total emitted E_{GW} is around $\sim 3 \times 10^{-10} M_{\odot}c^2$, the overall largest E_{GW} from anisotropic neutrino emission found for any presently published model.

Fryer et al. [179], also using gray flux-limited diffusion, but employing a 3D Newtonian smooth-particle hydrodynamics (SPH) scheme, studied four models with density perturbations of 25% to 40% in 30-degree wedges about the north pole. They found GW signals due to anisotropic neutrino emission with maximum amplitudes of the same order of magnitude as those reported by [123]. However, their signals exhibited much less time variation and a weaker burst associated with core bounce,

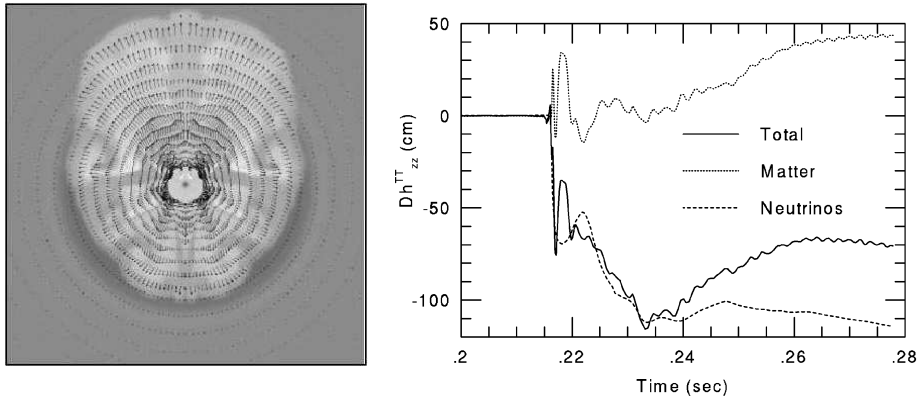


Figure 11. **Left:** Grey-scale map showing the entropy distribution ~ 50 ms into the explosion of the 2D asymmetric collapse model of Burrows and Hayes [123]. The physical scale is 4000×4000 km and velocity vectors are superposed. This plot corresponds to figure 1 of [123] and is used by kind permission from the authors. **Right:** GW signal due to anisotropic neutrino emission (dashed line), matter (dotted line) and combined matter+neutrinos (solid line) in the same model of [123]. This plot corresponds to figure 3 of [123] and is used by kind permission from the authors.

suggesting much lower energy emission (Fryer et al. did not provide values for E_{GW}).

9. Other GW Emission Mechanisms

9.1. Aspherical Outflows

Core-collapse SN explosions are unlikely to be perfectly spherically symmetric and all currently considered explosion mechanisms rely on the breaking of symmetry. Magnetically-driven explosions exhibit jet-like bipolar outflows (e.g., [17] and references therein), while explosions driven by the neutrino mechanism (e.g., [9]) or the acoustic mechanisms (e.g., [22]) can range from predominantly unipolar or bipolar outflows to nearly spherically symmetric explosions. In addition to the various explosion scenarios, precollapse large-scale asymmetries in the central regions of the star may also favor a largely asymmetric explosion.

The GW emission from rapid aspherical outflows has been considered by Obergaulinger et al. [90, 125] in the context of 2D magneto-rotational core collapse in Newtonian gravity and approximate GR (see section 3) and by Shibata et al. [117] in 2D GRMHD. Both groups of authors employed polytropic precollapse models, a simple polytropic + ideal gas (“hybrid”) EOS, and neglected neutrinos. At this level of approximation, the shock generally does not stall and a prompt explosion occurs after bounce.

Obergaulinger et al. and Shibata et al. both reported a quasi-monotonically growing contribution to the GW signal from bipolar outflows, leaving behind a GW memory akin that discussed in the context of GW emission from anisotropic neutrino radiation fields (see section 8). An example GW signal taken from the study of Obergaulinger et al. is shown in figure 12. Shibata et al. [117] pointed out that the GW signal systematics can be understood by considering an outflow of mass m in the z direction with slowly changing velocity. In this case, the contribution to the GW

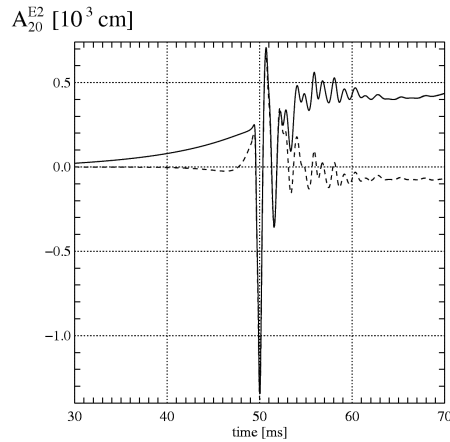


Figure 12. GW signal of the Obergaulinger et al. [90] model A1B3G3-D3M13 in terms of the quadrupole pure-spin Tensor harmonic amplitude A_{20}^{E2} , and $h_+ D = \frac{1}{8} \sqrt{\frac{15}{\pi}} \sin^2 \theta A_{20}^{E2}$. The dashed line gives the contributions of regions with radius $r \lesssim 60$ km while the solid line shows the total signal. The postbounce offset due to rapid aspherical outflows in the outer regions is clearly visible in the total signal. This figure corresponds to the lower-left panel of figure 8 in [90] and is used by kind permission from the authors.

signal by the outflow is $|h_{\text{out}}| \propto 2mv_z^2$. Once the outflow has reached a quasi-steady state, the mass ejection rate can be assumed to stay roughly constant, hence the mass in the outflow increases roughly linearly [17, 117]. Using this, the appropriate factors of G and c , and imposing a scaling on m and v_z , one finds [117]

$$|h_{\text{out},+}| D \approx 300 \left(\frac{m}{0.1 M_\odot} \right) \left(\frac{v_z}{0.1c} \right)^2 \text{ cm} . \quad (8)$$

Similar to the case of anisotropic neutrino emission, the slow variation of $|h_{\text{out},+}|$ leads to emission of only small E_{GW} that are emitted predominantly at low frequencies.

The approximate $|h_{\text{out},+}|$ given by equation 8 is in rough agreement (assuming $m = 0.1 M_\odot$ and $v_z = 0.1c$) with the GW memory amplitude of $\sim 6.5 \times 10^{-21}$ (at 10 kpc) that Shibata et al. found after ~ 15 ms of postbounce evolution in the most extreme model of their limited model set. Obergaulinger et al. [90, 125] performed a more extensive set of calculations, but did not publish the final GW signal memory amplitudes for all their models. Those that were shown in [90, 125] are in rough agreement with equation 8 and the results of Shibata et al. [117].

Finally, it is important to point out that the MHD-driven bipolar outflows observed in the microphysically-simple calculations of [90, 117, 125] occur very early (around ~ 5 – 20 ms) in the postbounce evolutions of their models. More realistic models computed by Burrows et al. [17] (who did not analyze the GW emission in their models) require of the order of ~ 100 ms to launch the bipolar outflow. This longer delay translates to lower accretion and mass expulsion rates and may result in smaller GW signal memory amplitudes than observed by [90, 117, 125] for their very early explosions.

9.2. Global Precollapse Asymmetries

Prior to core collapse and after silicon core burning has ceased, nuclear burning continues in convectively unstable silicon and oxygen burning shells at the outer edge of the iron core (see, e.g., [137]). The large- and small-scale density, composition and thermal perturbations induced by convection in these layers and at the outer edge of the iron core could become large [187, 220, 221, 222], perhaps up to $\sim 10\%$, and would essentially be frozen in during collapse [186].

The effect of these perturbations on the postbounce hydrodynamics depends on their magnitude and distribution. If they occur primarily on small scales and reach deep into the iron core, they may act as seeds for prompt and neutrino-driven convection (see section 6 for the associated GW signals). Larger-scale perturbations, on the other hand, can lead to strongly aspherical explosions into the direction of lowest density. Such largely aspherical ejection of matter – as just discussed in the previous section 9.1 – can lead to the burst emission of GWs with GW memory (e.g., [216, 223]) and, in the case of primarily unipolar outflow, may be responsible for pulsar birth kicks (e.g., [224, 225] and references therein).

Burrows & Hayes [123] were the first to perform a numerical study of core collapse with a globally asymmetric presupernova configuration. They employed an axisymmetric Newtonian code with gray flux-limited neutrino diffusion along rays. Their single model was a $15-M_{\odot}$ presupernova configuration perturbed by a 15% reduction of the density of the outer core within 20 degrees of its north pole. The left panel of figure 11 displays the aspherical explosion obtained in their model. It erupted preferentially through the lower-density polar regions and led to a recoil velocity of the PNS of ~ 530 km/s. The aspherical matter dynamics resulted in a GW burst signal (shown in figure 11) that set in ~ 5 ms after bounce and reached maximum amplitudes of $\sim 1 \times 10^{-21}$ (at 10 kpc) at early times with rapid time variation around ~ 500 Hz and an asymptotic memory of $\sim 1.5 \times 10^{-21}$ (at 10 kpc) built up over ~ 70 ms. The combined neutrino and matter GW signal exhibited a memory of $\sim 2.3 \times 10^{-21}$ (at 10 kpc) and the total emitted energy in GWs was $\sim 1.1 \times 10^{-9} M_{\odot} c^2$.

Fryer et al. [179, 226], using their 3D SPH scheme with gray flux-limited diffusion, performed a set of four calculations of a $15-M_{\odot}$ presupernova star. Three calculations were perturbed with an initial 30% to 40% density reduction in the oxygen and silicon layers in a 30-degree wedge centered about one of the poles. One calculation was set up with 25% lower density in a 30-degree polar wedge throughout iron core, silicon and oxygen shells. Despite the larger perturbations present in their models, Fryer et al. did not find strongly asymmetric explosions and reported neutron star kick velocities below ~ 200 km/s, arguing that momentum transfer by neutrinos was partly counteracting the hydrodynamic kick mechanism.

The GW emission from aspherical flow in the Fryer et al. models sets in within ~ 2 – 5 ms after bounce and, according to the authors, is mostly due to asymmetries caused by oscillations in the PNS core that are excited by the counteracting recoils due to aspherically ejected matter and neutrino momentum. However, h_+ and h_{\times} of their models show no periodicity and appear uncorrelated. Considering the discussion on prompt convection in section 6, it appears not unlikely that at least part of the GW signal is due to prompt convection. The GW signals reach their maximum amplitudes of ~ 2 – 8×10^{-22} (at 10 kpc) around 10–20 ms after bounce, decay thereafter and contain no large-amplitude GW memory. The absence of the latter is not discussed by Fryer et al., but may be due to the relatively small asphericity of their explosions.

The authors provided neither GW spectra nor numbers for the energy emitted in GWs.

9.3. Magnetic Fields

As already pointed out in section 8, not only aspherical matter dynamics, but any kind of accelerated transport of energy, including magnetic-field energy, may lead to the emission of GWs. Kotake et al. [87] extended the Newtonian quadrupole formalism of wave generation to include the contribution from magnetic fields and introduced terms associated with Lorentz force and magnetic-field energy. They focussed on the GW signal of rotating core collapse and bounce and performed a limited set of Newtonian 2D magneto-rotational core-collapse calculations with a finite-temperature nuclear EOS and a leakage scheme for neutrinos. They demonstrated that the magnetic contribution to the GW signal at core bounce remains smaller than $\sim 1\%$ of the matter contribution for cores with precollapse magnetization below $\sim 10^{12}$ G. The latter is already an extreme value, considering that garden-variety precollapse iron cores are likely to be weakly magnetized with $B \lesssim 10^7\text{--}10^{10}$ G [142]. Since matter and B-field are strongly coupled, the magnetic component of the GW signal exhibits time variations similar to those of the matter component. Interestingly, it leaves behind a secularly growing GW memory that, at 20 ms after bounce, dominates the overall signal with an amplitude of $\sim 2 \times 10^{-21}$ (at 10 kpc) in Kotake et al.'s model with precollapse magnetic field of 5×10^{12} G and central angular velocity $\Omega_{c,i} = 4 \text{ rad s}^{-1}$. This GW memory may be due to the gradual build-up of the magnetic field energy in polar regions via an Ω dynamo (e.g., [17, 90, 113] and references therein), but was not studied in detail by Kotake et al. Also note that the models of Kotake et al. were not followed through explosion, hence do not exhibit a contribution to the GW signal and GW memory from aspherical outflows (see section 9.1).

Obergaulinger et al. [90, 125] performed an extensive set of magneto-rotational core-collapse simulations with simplified microphysics, leading to prompt explosions with bipolar outflows (see section 9.1). They confirmed the previous result of Kotake et al. [87] that MHD effects on the dynamics and the magnetic contribution to the GW signal of core bounce remain small for cores with precollapse magnetic field strengths below $\sim 10^{12}$ G. For models with stronger precollapse magnetic fields, Obergaulinger et al. found significant magnetic contributions to the GW signal that grow after bounce due to the continuously increasing magnetic stresses in the polar regions and inside the PNS. The time variation in the magnetic component is much slower than in the matter component, peaking in frequency below ~ 100 Hz. In multiple models with strong magnetic fields (initial $B \gtrsim 10^{12}\text{--}10^{13}$ G), the magnetic component eventually dominates the GW signal and leaves behind a GW memory that may have positive or negative sign, varying from model to model. The maximum GW signal amplitudes due to the magnetic component generally scale with the precollapse magnetic field strength. For their most extreme model, Obergaulinger et al. found a maximum magnetic GW signal amplitude of $\sim 4.5 \times 10^{-21}$ (at 10 kpc) while most other models show one to two orders of magnitude smaller maximum amplitudes. Note that the GW memory due to the magnetic contribution linearly combines with the memory that is due to the bipolar outflow of matter. Depending on the sign of the magnetic contribution, the total amplitude of the GW memory may be increased or decreased.

9.4. GWs from Collapse to a Black Hole

Ordinary massive stars in the mass range from ~ 8 to $\sim 100 M_{\odot}$ burn their nuclear fuel all the way to iron-group nuclei (or a mixture of oxygen, neon, and magnesium nuclei at the lowest masses) and their cores stay in hydrostatic quasi-equilibrium throughout their nuclear burning lives. The final iron or ONeMg cores are supported primarily by the pressure of degenerate electrons (P_e), secondarily by the thermal pressure of the heavy ions (P_{ion}), and tertiarily by radiation pressure (P_{rad}) such that $P_e \gg P_{\text{ion}} \gg P_{\text{rad}}$ [4]. Hence, iron/ONeMg cores resemble white dwarfs and have effective Chandrasekhar masses in the range of ~ 1.3 to $\sim 2.0 M_{\odot}$ [3, 137]. When such a core collapses, it separates into a subsonically contracting inner core and a supersonically infalling and consequently rarefying outer core. At bounce, the inner core has a mass of ~ 0.5 to $\sim 0.7 M_{\odot}$ (depending on its average electron fraction Y_e , average specific entropy s , and rotational configuration [108, 143]). The solid-core of the nuclear force and the resulting stiff EOS above nuclear density *easily* stabilizes the collapse of the inner core. Collapse *always* results in a PNS and direct collapse to a black hole (BH) without core bounce and a PNS phase *occurs never* in ordinary massive stars[¶].

After bounce, outer core material accretes onto the PNS. The maximum baryonic NS mass[†] that can be supported against gravity depends sensitively on the stiffness of the high-density EOS and ranges between $\sim 1.5 M_{\odot}$ and $\sim 2.5 - 3 M_{\odot}$ (e.g., [5, 228, 229]). Rapid differential rotation can enhance the maximum mass by up to $\sim 50\%$ (e.g., [230]), while the thermal structure of the PNS has less influence on the maximum mass [229, 231].

In order to leave behind a neutron star, the SN explosion has to set in before the PNS has reached its maximum mass. Depending on the latter's actual value and on the accretion rate set by the structure of the progenitor, an explosion has to occur within $\sim 1 - 2$ s after bounce. If the explosion is weak and does not unbind the entire stellar envelope, fall-back accretion can still push the PNS over its mass limit at later times (e.g., [232]). When a PNS becomes gravitationally unstable before the explosion is launched, the SN engine is immediately shut off and the star ends its life as a collapsar, possibly exploding in a gamma-ray burst if it possesses the needed amount and distribution of angular momentum [19, 20, 233].

Nonspherical PNS collapse to a BH results in a burst of GWs (1) due to the rapidly shrinking mass-quadrupole moment of the PNS during the collapse and (2) due to the quasi normal mode (QNM) ringing of the nascent BH that is initially distorted from its stationary Kerr shape and experiences subsequent distortion by accreting material.

The GW emission from the collapse of a compact star to a BH was first considered in the late 1970's by Cunningham, Price, and Moncrief [234, 235, 236] whose work was later improved by Seidel and collaborators [237, 238] and more recently by Harada, Iguchi, and Shibata [239]. These authors employed a perturbative approach and studied the GW emission from nonspherical perturbations on a spherically-symmetric background. They found that the overall GW signal of BH formation is dominated by

[¶] There is considerable confusion in the astrophysics community about this fact. This is in part due to the misleading use of the terms 'direct/prompt BH formation' and 'delayed BH formation' by Fryer, Woosley, and collaborators. In their context (e.g., [227]), these terms describe 'BH formation without SN explosion' and 'BH formation after SN explosion by fallback accretion', respectively.

[†] Astronomical observations generally measure the gravitational mass, the baryonic mass minus the mass-energy equivalent of the NS gravitational binding energy.

the QNM ringing of the formed BH and that most of the GWs are emitted from the fundamental quadrupole mode. If the perturbation is axisymmetric (i.e., primarily due to rotation) the emission is dominated by the $\ell = 2, m = 0, n = 0$ (200) multipolar component, while nonaxisymmetric perturbations show up as $\ell = 2, m \neq 0, n = 0$ modes. These modes emit at characteristic frequencies that depend only on the BH mass M and its dimensionless angular momentum parameter $j = (cJ)/(GM^2)$. Berti et al. [240] provide fitting-formulae and coefficients that describe to better than $\sim 5\%$ accuracy the BH QNM frequencies f_{lmn} . Focussing on the 200 (axisymmetric) and 220 (nonaxisymmetric, bar-like) QNMs, we find using their tables,

$$f_{200} = 14.4 \left(\frac{M}{M_\odot} \right)^{-1} (1 - 0.165(1 - j)^{0.355}) \text{ kHz} , \quad (9)$$

$$f_{220} = 49.4 \left(\frac{M}{M_\odot} \right)^{-1} (1 - 0.759(1 - j)^{0.1292}) \text{ kHz} . \quad (10)$$

Hence, a nonrotating BH with a mass of $2 M_\odot$ rings when perturbed in its 200 (or 220) mode with a frequency of ~ 6 kHz and this frequency decreases linearly as more matter is accreted. In the case of slow rotation (small j), one would expect a 'reverse chirp' from higher to lower frequencies in the GW signal as a BH is formed and accretes the massive stellar envelope in a failing core-collapse SN. With increasing spin, the QNM frequencies increase at different rates for different azimuthal mode number m and for rapid rotation, the decrease of the QNM frequencies by increasing BH mass could be partly compensated by increasing j . Initial and advanced LIGO-class detectors have their maximum sensitivity at frequencies below ~ 1 kHz, thus will require large signal amplitudes and emitted energies to detect even a galactic NS collapse event.

By making estimates of the energy in the perturbations and its azimuthal m distribution, one can use equations 9 and 10 and analogous expressions for other m to estimate GW signal amplitudes. This can be done as outlined in [88] or by assuming that the GW signal is of sine-Gaussian shape as discussed, e.g., in [243]. However, this shall not be repeated here, since such estimates for spatial distribution and energy of perturbations cannot be made reliably. The latter highlights a fundamental problem of the perturbative approach: While the effects of a (small) perturbation on a background can be studied with great accuracy, the perturbation itself cannot be determined and must be put in by hand or provided as initial data from numerical simulations (e.g., [244]).

Direct numerical simulation of nonspherical BH formation using GR hydrodynamics coupled to spacetime curvature evolution allows for the self-consistent determination of the GW signal. The first 2D simulations of BH formation were carried out in 1981 by Nakamura [245], but GWs could not be extracted due to numerical difficulties. The first waveforms and GW energy estimates from axisymmetric rotating stellar collapse to a BH were provided in 1985 by Stark and Piran [246] who used highly approximate initial data that were not in rotational equilibrium. More recently, Baiotti et al. [241, 242] presented the first GW signals from the 3D collapse of rigidly-rotating polytropic NS models in rotational equilibrium. They found that a collapsing rotating NS stays essentially axisymmetric and confirmed that the GW emission is primarily due to axisymmetric BH QNM oscillations. They also identified a high-frequency, pre-BH formation component that is sensitive to the way the collapse of the polytropic NS is instigated. In figure 13, we present the GW signal (left panel) and GW power spectrum of the QNM ringing (right panel) extracted

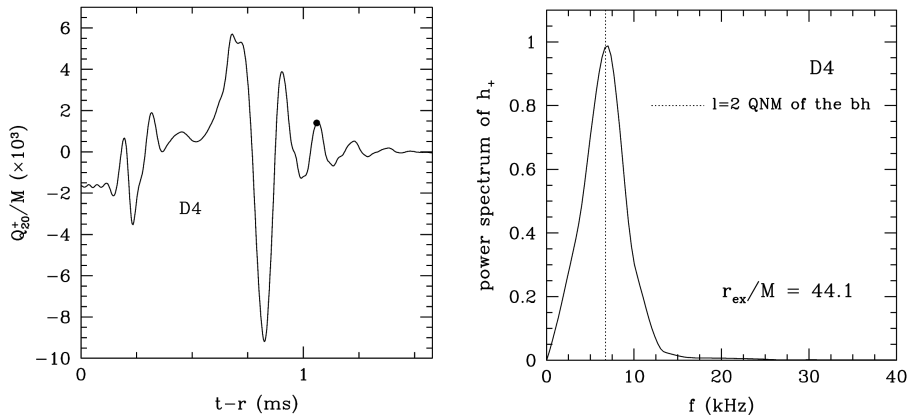


Figure 13. **Left:** GW signal of the collapse of a rapidly rigidly rotating polytropic NS to a black hole in terms of the dominant even-parity metric perturbation Q_{20}^+ as computed by Baiotti et al [241, 242]. Even-parity and odd-parity metric perturbations are related to the two physical GW polarizations according to $h_+ - ih_\times = \frac{1}{2D} \sum_{l,m} (Q_{lm}^+ - i \int_{-\infty}^t Q_{lm}^\times dt') {}_{-2}Y^{lm}$, where ${}_{-2}Y^{lm}$ is the -2 spin-weighted spherical harmonic [122, 241]. This plot corresponds to the bottom-right panel of figure 5 of [242] and is used by kind permission from the authors. **Right:** Power spectrum of the BH ring-down part of the GW signal for the same model the units are chosen in such a way that the peak of the power spectrum is approximately 1. The dotted line marks the BH QNM frequency obtained by perturbation theory. This plot corresponds to the bottom-right panel of figure 6 of [242] and is used by kind permission from the authors.

from the rapidly rigidly rotating collapse model D4 with $M = 1.86 M_\odot$ and $j = 0.54$ of Baiotti et al. [242]. While the early part of the waveform is dominated by details of the matter dynamics and may be sensitive to the EOS and the NS angular momentum distribution, the BH QNM ringing depends only on the mass M and angular momentum parameter j , hence, will be qualitatively and quantitatively similar in simulations that take into account a more realistic matter treatment and differential rotation. For their model suite, Baiotti et al. [241, 242] give a maximum energy emission of $E_{\text{GW}} = 1.45 \times 10^{-6} (M/M_\odot) M_\odot c^2$ which obtains in their most rapidly rotating model D4 and scales roughly as j^4 at small j . Convolving their GW signals with detector noise curves as discussed in [34], they find an upper-limit characteristic strain h_c of $\sim 5.5 \times 10^{-22} (M/M_\odot)$ at 10 kpc and at a characteristic frequency f_c of ~ 530 Hz for initial LIGO detectors. These numbers suggest that BH formation in a galactic core-collapse event with rapid rotation may be marginally detectable already with initial LIGO-class detectors.

Simulations that track BH formation in a microphysically detailed multi-D model of a failing core-collapse SN remain to be carried out. Such simulations are necessary for the self-consistent study of the early, pre-QNM ringing GW signal of PNS collapse as well as for the GW signal of BH QNM oscillations excited by long-term accretion (but see [247] for a perturbative treatment of the latter).

Table 4. List of optically discovered core-collapse SNe that occurred within 5 Mpc from Earth between January 1, 2002 and August 31, 2008. The table is based on the comprehensive online SN listing at <http://www.cfa.harvard.edu/iau/lists/Supernovae.html>. Given are the SN name, the name of the host galaxy, the date of discovery, the core-collapse SN spectral subtype (see, e.g., [250]), and the approximate distance. Note that the date of astronomical discovery always postdates the actual explosion.

SN	Host Galaxy	Date	Type	Distance
2008bk	NGC 7793	20080325 [251]	II-P	~ 3.9 [252]
2005af	NGC 4945	20050208 [253]	II-P	~ 3.6 [252]
2004dj	NGC 2403	20040731 [254]	II-P	~ 3.3 [252]
2004am	M 82	20040305 [255]	II-P	~ 3.5 [256]
2002kg	NGC 2403	20021026 [257]	IIn	~ 3.3 [252]

10. Nearby Core-Collapse SNe, the recent SN 2008bk, and their Detectability in Gravitational Waves

Optimistic estimates of the core-collapse SN rate in the Milky Way and the close-by Small and Large Magellanic Clouds predict one core-collapse SN in $\sim 30 - 50$ years and even for the entire local group of galaxies, including M31 at 0.8 Mpc, one core-collapse SN in ~ 20 years is an optimistic estimate (see, e.g., [37] and the compilation of rate estimates and references in [42]). This rate stays roughly constant until a distance of ~ 3 Mpc. The galaxies of the M81 group and neighboring groups with high star-formation rates that are located at 3–5 Mpc from Earth increase the core-collapse SN rate to an optimistic 1 core-collapse SN in ~ 2 years within ~ 5 Mpc [38, 248]. The next significant increase in the SN rate occurs when the outskirts of the Virgo cluster are beginning to contribute at 7–10 Mpc [38].

Since LIGO/GEO600 [26, 27] science operations began in 2002, five core-collapse SNe have been discovered optically within 5 Mpc from Earth, a number roughly consistent with the above quoted rate estimate. Unfortunately, all events occurred outside of LIGO/GEO600 and VIRGO [28] science runs. However, the very recent (as of August 2008) nearby core-collapse SN, SN 2008bk, occurred while GEO600 and the 2-km LIGO Hanford interferometer (H2) were taking data in “astrowatch” mode [249]. All other LIGO-class detectors, including VIRGO, were offline for upgrades.

SN 2008bk was found on March 25, 2008 in NGC 7793 [251], a spiral galaxy, approximately 3.9 Mpc away from Earth. Based on the lightcurve evolution of similar type II-P (“plateau,” see, e.g., [250]), 2008bk exploded $\sim 20 - 36$ days before its discovery [251]. The progenitor star appears to have been on the low-mass end of the massive-star population and may have had a mass between $8.5 \pm 1 M_{\odot}$ [258, 259].

Since LIGO H2 and GEO600 were most likely taking data when SN 2008bk exploded, it is interesting to estimate the detectability by H2 and GEO600 for the GW emission mechanisms discussed in in this review. Given the high rate of core-collapse SNe between ~ 3 and ~ 5 Mpc it is also useful to consider their detectability by other current and future GW observatories.

Since waveforms for some of the GW emission mechanisms are available, we compute single-detector optimal (assuming perfect orientation) matched-filtering signal-to-noise ratios (SNR), using

$$(\text{SNR})_{\text{optimal}}^2 = 4 \int_0^{\infty} \frac{|\tilde{h}_+(f)|^2 + |\tilde{h}_{\times}(f)|^2}{S(f)} df, \quad (11)$$

Table 5. Upper-limit SNR estimates for SN 2008bk at 3.9 Mpc using theoretical noise power spectral densities for advanced LIGO 4-km interferometers (LIGO 2 4km), LIGO 1 4-km interferometers (LIGO L1/H1), VIRGO, and LIGO S5 data for the H2 and GEO600 interferometers. Considered are various representative models for GW emission by rotating core collapse and bounce, nonaxisymmetric rotational instabilities, and PNS core g -modes. Behind each model name a paper reference is provided. For some models, \sqrt{n} -scaled SNRs are given as estimates for longer GW emission than tracked by the model calculations. This is denoted by ($\times n$) behind the model name.

Process	Model	LIGO 2 4 km	LIGO L1/H1 4 km	LIGO H2 2 km	GEO600 600 m	VIRGO 3 km
Rotating Collapse & Bounce [108]	s11A2O13	0.124	0.008	0.005	0.001	0.009
	s20A2O09	0.130	0.008	0.006	< 0.001	0.010
	s40A3O12	0.214	0.024	0.013	< 0.001	0.018
Rotational Instability [42, 115, 119]	s20A2B4	0.319	0.021	0.014	0.003	0.022
	s20A2B4 ($\times 5$)	0.713	0.047	0.031	0.007	0.049
PNS g -modes [22, 23] and section 7.1	s11.2	0.147	0.006	0.005	0.002	0.009
	s15.0	0.454	0.021	0.015	0.006	0.027
	s25.0	0.612	0.029	0.020	0.007	0.037
	s25.0 ($\times 2$)	0.866	0.041	0.029	0.009	0.052
	s25WW	5.331	0.217	0.151	0.057	0.328

where $S(f)$ is the one-sided detector noise power spectral density in units of $\text{Hz}^{-1/2}$ and \tilde{h} is the Fourier transform of the wave signal, computed via [34, 191]

$$\tilde{h}_{+, \times}(f) = \int_{-\infty}^{\infty} e^{2\pi i f t} h_{+, \times}(t) dt . \quad (12)$$

Using the characteristic strain $h_{\text{char}}(f)$ defined by equation 2, equation 11 can be rewritten [191] to

$$(\text{SNR})_{\text{optimal}}^2 = \int_0^{\infty} d \ln f \frac{h_{\text{char}}^2(f)}{h_{\text{rms}}^2(f)} , \quad (13)$$

where $h_{\text{rms}}(f)$ is the dimensionless detector rms noise given by $h_{\text{rms}}(f) = \sqrt{fS(f)}$. Note that the expression for the optimal SNR given here is a factor of 3/2 smaller than the expression used in [108] and derived in [34]. See [191] for details.

For computing $\text{SNR}_{\text{optimal}}$, we employ noise power spectral densities $S(f)$ for H2 and GEO600 from the LIGO/GEO600 S5 runs. The H2 $S(f)$ data have so far not been published and were kindly made available to us by M. Landry [260]. The GEO600 $S(f)$ data were obtained from the GEO600 website [27]. In addition, we compute $\text{SNR}_{\text{optimal}}$ based on the design $S(f)$ for VIRGO [28], LIGO Livingston/Hanford 1 [190], and advanced LIGO 4-km interferometers (LIGO 2) in burst mode [190].

In table 5, we list $\text{SNR}_{\text{optimal}}$ for all considered detectors and for models focussing on GW signals from rotating collapse and bounce, nonaxisymmetric rotational instabilities, and PNS g -modes at the distance of SN 2008bk. GW emission from convective overturn and the other emission mechanisms considered in this review are not included in table 5, since their $\text{SNR}_{\text{optimal}}$ would be of order 10^{-3} and below at a distance of ~ 4 Mpc even for advanced LIGOs (see, e.g., [97] and sections 6 and 9).

The first model given for each emission process in table 5 is an ‘‘average emitter’’ and the subsequent models range from ‘‘strong’’ to ‘‘extreme’’. Since in many computed models the simulation was stopped before the GW emission had subsided,

we also provide \sqrt{n} -scaled (where n is the factor by which the emission is prolonged) $\text{SNR}_{\text{optimal}}$ for a subset of models.

Based on the $\text{SNR}_{\text{optimal}}$ listed in table 5, we surmise that LIGO H2 and GEO600 had no chance of seeing GWs emitted in SN 2008bk. Even the most extreme models yield optimal SNRs below ~ 0.2 at a source distance of 3.9 Mpc. For a detection, a SNR significantly greater than 1 and probably in the range of 5 – 7 would be needed (e.g., [97, 191]). Once in operation and at design sensitivity, advanced LIGO could constrain the GW emission from PNS g -modes out to the distance of SN 2008bk and beyond. All other emission processes require a closer core-collapse event (or more sensitive future detectors) to be observable.

11. Putting things together: Summary and a Conjecture

The GW signature of core-collapse SNe is rich and multi-faceted. The aim of this review was to provide an overview and summary of the current knowledge about the various GW emission processes that may occur in a core-collapse event.

We have outlined and discussed rotating core collapse and bounce, nonaxisymmetric rotational instabilities, postbounce convective overturn, and non-radial PNS pulsations as the prominent candidate processes whose multi-D dynamics are likely to emit GWs. In addition, we have summarized the emission characteristics of the GW signals associated with anisotropic neutrino emission, aspherical outflows, magnetic stresses, global precollapse asymmetries, and the collapse of hypermassive PNSs to BHs.

All of the listed processes are burst emitters of GWs, but range in temporal and spectral characteristics from short, few-ms bursts with rather narrow-band emission (e.g., rotating collapse and bounce) to broadband emission lasting, perhaps, for seconds (e.g., convection, in particular PNS convection). In addition, a number of the emission processes produce bursts with GW memory, leaving behind essentially zero-frequency, permanent distortions of spacetime.

Rotating core collapse and bounce is the most extensively investigated and arguably the best understood source of GWs in the core collapse context. 2D and 3D simulations in conformally-flat and full GR were carried out and included the dominant microphysical aspects, results of different approaches agree, and waveform catalogs are available [126, 155] to the GW data analysis community which is beginning to employ them (e.g., [261, 262]). Nevertheless, uncertainties remain. Without doubt, the biggest is the lack of presupernova models from multi-D stellar evolution simulations. Present simulations have to rely upon profiles from 1D stellar evolution codes that take into account crucial multi-D effects such as convection and rotation in only highly approximate ways. Core collapse investigations try to deal with this by large-scale parameter studies, but until multi-D stellar evolution models become available and reliable, even extensive parameter studies could, in principle, be missing the real precollapse configurations that obtain in nature.

In order to produce a burst of GWs at core bounce comfortably detectable by advanced LIGOs throughout the Milky Way, a precollapse iron core needs ([108] and section 4) to be spinning very rapidly with central periods $P_o \lesssim 6$ s (corresponding to central angular velocities $\Omega_o \gtrsim 1$ rad s⁻¹). Initial LIGOs might see cores with $P_o \lesssim 3$ s. Perhaps only $\sim 1\%$ or less of the massive star population rotates with such short periods at the onset of core collapse [144], while the vast majority is likely

spinning much more slowly with periods of 30 – 100 s as currently predicted [141, 142].

Rapidly spinning iron cores with the above stated short central periods produce millisecond-period PNSs with rotational energy of order 10^5 B of which a fraction would be sufficient to power an energetic SN explosion. Moreover, such PNSs have strongly differentially-rotating outer cores (e.g., [108, 141, 263]) and are likely to become subject to nonaxisymmetric rotational instabilities which would lead to the GW emission characteristics outlined in section 5. As discussed by a number of groups (e.g., [16, 17, 20, 90, 117, 165]), magnetic field amplification can draw from rotational energy. In particular, Burrows et al. [17] found that cores with $P_0 \lesssim 2 - 4$ s develop MHD-driven jet-like SN explosions*. Hence, there is a close link between a detectable GW burst from core bounce and MHD-driven explosions. The same may be true for 3D rotational instabilities and their GW signal, but it is presently not known in which way 3D hydrodynamic and MHD instabilities interact in a postbounce SN core.

Convection and the SASI are very likely to be present in the postbounce pre-explosion phase of the vast majority of core-collapse events. Rapid rotation damps convection and a very early onset of explosion, probably relevant only in the case of ONeMg cores in the lowest-mass massive stars [2, 12], can shut off convection before it is fully developed.

In contrast to the GW signal of rotating collapse and bounce, the GW emission characteristics of postbounce convective overturn and the SASI have been investigated by only a few studies and the systematics of the GW signal with variations in progenitor structure, rotational configuration etc. have not been investigated in detail. Furthermore, owing to the stochastic nature of both large-eddy and small-scale turbulent convection, GW templates that could be expected to match real signals cannot be predicted. It will most likely take an advanced LIGO-class detector to detect for a galactic event the broadband $\sim 0.5 - 1.5$ s GW signal emitted by convection/SASI before explosions and the longer-duration, but lower-amplitude GW signal from PNS convection.

The explosion scenario currently favored for slowly rotating and nonrotating massive stars – the neutrino mechanism (e.g., [2, 4, 7]) – relies on the deposition of sufficient energy by neutrinos in the postshock region to revive the stalled shock and unbind the stellar envelope. A multitude of multi-D simulations have demonstrated that convection and SASI are key ingredients for neutrino-driven core-collapse SN explosions (e.g., [9, 10] and references therein). The acoustic mechanism, recently proposed by Burrows et al. [21, 22] and intensely debated in the community [9, 24, 25], is an alternative to the neutrino mechanism and relies on the excitation by accretion and turbulence of large-amplitude PNS core g -modes and their damping by strong sound waves that deposit energy in the postshock region, eventually leading to explosion. The GW signature of an acoustically-driven core-collapse SN explosion would be dominated by the GWs emitted from the quadrupole components of the PNS core pulsations. Already first-generation LIGOs should be able to see such a strong signal throughout the Milky Way. Advanced detectors may be able to put significant constraints on the signal strength out to 3 – 5 Mpc where the SN rate is favorably high.

In table 6 we summarize the prominent GW emission processes that are expected to be active in a core-collapse event and contextualize them with the three core-collapse

* Provided either that the magneto-rotational instability (MRI) [164] occurs as envisioned or that the precollapse core magnetic field is at least of the order of 10^{11} G.

Table 6. Overview on prominent GW emission processes in core-collapse SNe and their possible emission ‘levels’ in the context of the magneto-rotational (MHD; e.g. [17]), the neutrino (e.g., [9]), and the acoustic SN mechanism (e.g., [21, 22]). For a *galactic* SN, ‘strong’ corresponds to ‘probably detectable by initial and advanced LIGO’, ‘weak’ means ‘probably marginally detectable by advanced LIGO’, and ‘none’ means ‘absent or probably not detectable by advanced LIGO’. The three considered explosion mechanisms are likely to have mutually exclusive GW signatures and could be distinguished by the mere detection or non-detection of a GW signal without the solution of the full inverse problem. Note that the GW signal due to anisotropic neutrino emission, though present in all three mechanism, is not considered, since its low-frequency character severely limits its detectability.

GW Emission Process	Potential Explosion Mechanism		
	MHD Mechanism (rapid rotation)	Neutrino Mechanism (slow/no rotation)	Acoustic Mechanism (slow/no rotation)
Rotating Collapse and Bounce	strong	none/weak	none/weak
3D Rotational Instabilities	strong	none	none
Convection & SASI	none/weak	weak	weak
PNS <i>g</i> -modes	none/weak	none/weak	strong

SN explosion mechanisms by semi-quantitatively assigning ‘emission strengths’ for a galactic event ($D \approx 10$ kpc) based on the GW emission estimates collected in this review. In the scale we assume, ‘none’ refers to ‘absent or probably not detectable by advanced LIGOs ($\text{SNR} \ll 1$)’, ‘weak’ means ‘probably only marginally detectable by advanced LIGOs ($\text{SNR} \gtrsim 1$)’, ‘strong’ reflects ‘probably detectable by initial and advanced LIGOs ($\text{SNR} \gtrsim 5 - 7$).’ The roughness of the scale is intended to emphasize the independence of the overall argument from variations in quantitative details.

The MHD mechanism is limited to rapidly rotating cores, hence will involve strong GW emission from core bounce and, perhaps, nonaxisymmetric rotational instabilities. The acoustic mechanism, on the other hand, may work best in nonrotating or slowly rotating cores and will emit a strong GW signal from PNS pulsations. The neutrino mechanism, also probably most relevant in slowly or nonrotating cores, will very likely have convection/SASI as its strongest source of GWs.

Based on the above discussion and on table 6, we conjecture that *the GW signatures of the neutrino, MHD, and acoustic core-collapse SN mechanisms are mutually exclusive*. Hence, for a galactic SN and even initial LIGOs, the mere detection of a GW signal and its association with an emission process and, in fact, also the non-detection of GWs, have the potential of strongly constraining the way massive stars explode.

Unfortunately, galactic core-collapse SNe are quite rare events, occurring at a rate of one in a few decades. Initial LIGO-class detectors cannot see core-collapse SNe outside the Milky Way. Advanced detectors, at least as currently planned [190], may be able to see most core-collapse SNe throughout the local group of galaxies ($D \approx 1$ Mpc). This, however, would increase the observable event rate by not more than a factor of ~ 2 [37, 38]. Third-generation GW observatories (e.g. the envisioned

EURO detector [264]) reaching out to at least 3 – 5 Mpc will be necessary for detailed GW astronomy of core-collapse SNe to become possible.

Acknowledgements

The author wishes to thank A. Burrows, L. Lehner, and B. Schutz for encouraging him to write this topical review. The author is indebted to his collaborators A. Burrows, L. Dessart, E. Livne, and J. Murphy for letting him use previously unpublished theoretical GW signal data in this article. He also thanks K. Kotake for providing him with the derivation of equation 7 and for helpful exchanges. Furthermore, the author finds it a pleasure to acknowledge helpful discussions with S. Akiyama, S. Ando, E. Berti, A. Burrows, A. Calder, P. Cerdá-Durán, L. Dessart, H. Dimmelmeier, L. S. Finn, H.-T. Janka, E. Katsavounidis, M. Landry, A. Marek, T. Marquart, M. Marschall, R. O’Shaughnessy, E. Müller, J. Murphy, E. O’Connor, B. Schutz, E. Seidel, E. Schnetter, K. S. Thorne, and L. Wen. Part of this work was carried out during the Gravitational Wave Astronomy Workshop at the Aspen Center of Physics, May-June 2008. This work was supported by a Joint Institute for Nuclear Astrophysics postdoctoral fellowship, sub-award no. 61-5292UA of NFS award no. 86-6004791 at the University of Arizona, by a Sherman Fairchild postdoctoral fellowship at Caltech, by an Otto Hahn Prize awarded to the author by the Max Planck Society, and by a research fellowship from the Albert Einstein Institute.

References

- [1] A. Burrows. *Nature*, **403**, 727, 2000.
- [2] H.-T. Janka, K. Langanke, A. Marek, G. Martínez-Pinedo, and B. Müller. *Phys. Rep.* , **442**, 38, 2007.
- [3] E. Baron and J. Cooperstein. *Astrophys. J.*, **353**, 597, 1990.
- [4] H. A. Bethe. *Rev. Mod. Phys.*, **62**, 801, 1990.
- [5] J. M. Lattimer and M. Prakash. *Phys. Rep.* , **442**, 109, 2007.
- [6] A. Burrows, L. Dessart, C. D. Ott, and E. Livne. *Phys. Rep.* , **442**, 23, 2007.
- [7] H. A. Bethe and J. R. Wilson. *Astrophys. J.*, **295**, 14, 1985.
- [8] R. Buras, H.-T. Janka, M. Rampp, and K. Kifonidis. *Astron. Astrophys.* , **457**, 281, 2006.
- [9] A. Marek and H.-T. Janka. *Submitted to Astrophys. J. ArXiv e-prints, 0708.3372 [astro-ph]*, 2007.
- [10] J. W. Murphy and A. Burrows. *Astrophys. J. in press. ArXiv e-prints 0805.3345 [astro-ph]*, 2008.
- [11] L. Scheck, H.-T. Janka, T. Foglizzo, and K. Kifonidis. *Astron. Astrophys.* , **477**, 931, 2008.
- [12] A. Burrows, L. Dessart, and E. Livne. The Multi-Dimensional Character and Mechanisms of Core-Collapse Supernovae. In S. Immler and R. McCray, editors, *AIP Conference Series*, volume 937, page 370, 2007.
- [13] F. S. Kitaura, H.-T. Janka, and W. Hillebrandt. *Astron. Astrophys.* , **450**, 345, 2006.
- [14] J. M. LeBlanc and J. R. Wilson. *Astrophys. J.*, **161**, 541, 1970.
- [15] E. M. D. Symbalisty. *Astrophys. J.*, **285**, 729, 1984.
- [16] S. Yamada and H. Sawai. *Astrophys. J.*, **608**, 907, 2004.
- [17] A. Burrows, L. Dessart, E. Livne, C. D. Ott, and J. Murphy. *Astrophys. J.*, **664**, 416, 2007.
- [18] H. Sawai, K. Kotake, and S. Yamada. *Astrophys. J.*, **672**, 465, 2008.
- [19] S. E. Woosley and J. S. Bloom. *Ann. Rev. Astron. Astrophys.*, **44**, 507, 2006.
- [20] L. Dessart, A. Burrows, E. Livne, and C. D. Ott. *Astrophys. J. Lett.*, **673**, L43, 2008.
- [21] A. Burrows, E. Livne, L. Dessart, C. D. Ott, and J. Murphy. *Astrophys. J.*, **640**, 878, 2006.
- [22] A. Burrows, E. Livne, L. Dessart, C. D. Ott, and J. Murphy. *Astrophys. J.*, **655**, 416, 2007.
- [23] C. D. Ott, A. Burrows, L. Dessart, and E. Livne. *Phys. Rev. Lett.*, **96(20)**, 201102, 2006.
- [24] S. Yoshida, N. Ohnishi, and S. Yamada. *Astrophys. J.*, **665**, 1268, 2007.
- [25] N. N. Weinberg and E. Quataert. *Mon. Not. Roy. Astron. Soc.* , **387**, L64, 2008.
- [26] URL <http://ligo.caltech.edu>. LIGO.

- [27] URL <http://geo600.aei.mpg.de>. GEO600.
- [28] URL <http://www.virgo.infn.it>. VIRGO.
- [29] URL <http://tamago.mtk.nao.ac.jp>. TAMA300.
- [30] P. Astone et al. *Phys. Rev. D.*, **76**(10), 102001, 2007.
- [31] URL <http://www.minigrail.nl>. MiniGRAIL.
- [32] URL <http://www.das.inpe.br/graviton/english.html>. Mário Schenberg Gravitational Wave Detector.
- [33] S. E. Whitcomb. *Class. Quant. Grav.*, **25**(11), 114013, 2008.
- [34] K. S. Thorne. In S. W. Hawking and Israel W., editors, *300 Years of Gravitation*, Cambridge, UK, 1987. Cambridge University Press.
- [35] K. Kotake, K. Sato, and K. Takahashi. *Rep. Prog. Phys.*, **69**, 971, 2006.
- [36] C. Fryer and K. C. B. New. *Liv. Rev. Rel.*, **6**, 2, 2003.
- [37] S. van den Bergh and G. A. Tammann. *Ann. Rev. Astron. Astroph.*, **29**, 363, 1991.
- [38] S. Ando, F. Beacom, and H. Yüksel. *Phys. Rev. Lett.*, **95**, 171101, 2005.
- [39] R. Mönchmeyer, G. Schäfer, E. Müller, and R. Kates. *Astron. Astrophys.*, **246**, 417, 1991.
- [40] T. Zwerger and E. Müller. *Astron. Astrophys.*, **320**, 209, 1997.
- [41] C. D. Ott, A. Burrows, E. Livne, and R. Walder. *Astrophys. J.*, **600**, 834, 2004.
- [42] C. D. Ott. *Stellar Iron Core Collapse in 3+1 General Relativity and The Gravitational Wave Signature of Core-Collapse Supernovae*. PhD thesis, Universität Potsdam, Potsdam, Germany, 2006. URL <http://nbn-resolving.de/urn/resolver.pl?urn=urn:nbn:de:kobv:517-opus-12986>.
- [43] M. Shibata and Y.-I. Sekiguchi. *Phys. Rev. D.*, **68**(10), 104020, 2003.
- [44] L. Baiotti, S. Bernuzzi, G. Corvino, R. De Pietri, and A. Nagar. *arXiv:0808.4002 [gr-qc]*, 2008.
- [45] A. Einstein. *Preuss. Akad. Wiss. Berlin, Sitzber.*, page 154, 1918.
- [46] H. Bondi. *Nature*, **179**, 1072, 1957.
- [47] D. M. Eardley. Theoretical models for sources of gravitational waves. In N. Deruelle and T. Piran, editors, *Gravitational Radiation*, page 257, Amsterdam, 1983. North-Holland.
- [48] J. Weber. *Phys. Rev. Lett.*, **117**, 306, 1960.
- [49] J. Weber. *Phys. Rev. Lett.*, **17**, 1228, 1966.
- [50] F. J. Dyson. *Gravity Research Foundation Prize Essays*, 1962.
- [51] R. Ruffini and J. A. Wheeler. Relativistic Cosmology and Space Platforms. In V. Hardy and H. Moore, editors, *Proceedings of the Conference on Space Physics, ESRO, Paris, France*, page 45, 1971.
- [52] J. A. Wheeler. *Ann. Rev. Astron. Astroph.*, **4**, 393, 1966.
- [53] J. M. Bardeen, K. S. Thorne, and D. W. Meltzer. *Astrophys. J.*, **145**, 505, 1966.
- [54] D. W. Meltzer and K. S. Thorne. *Astrophys. J.*, **145**, 514, 1966.
- [55] K. S. Thorne and A. Campolattaro. *Astrophys. J.*, **149**, 591, 1967.
- [56] R. Price and K. S. Thorne. *Astrophys. J.*, **155**, 163, 1969.
- [57] K. S. Thorne. *Astrophys. J.*, **158**, 1, 1969.
- [58] K. S. Thorne. *Astrophys. J.*, **158**, 997, 1969.
- [59] A. Campolattaro and K. S. Thorne. *Astrophys. J.*, **159**, 847, 1970.
- [60] K. Kokkotas and B. Schmidt. *Liv. Rev. Rel.*, **2**, 2, 1999.
- [61] N. Andersson. *Class. Quant. Grav.*, **20**, 105, 2003.
- [62] T. X. Thuan and J. P. Ostriker. *Astrophys. J. Lett.*, **191**, L105, 1974.
- [63] I. D. Novikov. *Soviet Astron.*, **52**, 657, 1975.
- [64] S. L. Shapiro. *Astrophys. J.*, **214**, 566, 1977.
- [65] R. A. Saenz and S. L. Shapiro. *Astrophys. J.*, **221**, 286, 1978.
- [66] R. A. Saenz and S. L. Shapiro. *Astrophys. J.*, **229**, 1107, 1979.
- [67] R. A. Saenz and S. L. Shapiro. *Astrophys. J.*, **244**, 1033, 1981.
- [68] R. Epstein. *The post-Newtonian theory of the generation of gravitational radiation and its application to stellar collapse*. PhD thesis, Stanford University, Stanford, USA, 1976.
- [69] V. Moncrief. *Astrophys. J.*, **234**, 628, 1979.
- [70] S. Detweiler and L. Lindblom. *Astrophys. J.*, **250**, 739, 1981.
- [71] C.-W. Chin. *Phys. Rev.*, **139**, 761, 1965.
- [72] W.-Y. Chau. *Astrophys. J.*, **147**, 664, 1967.
- [73] S. Chandrasekhar. *Astrophys. J.*, **161**, 571, 1970.
- [74] B. D. Miller. *Astrophys. J.*, **187**, 609, 1974.
- [75] J. R. Ipser and R. A. Managan. *Astrophys. J.*, **282**, 287, 1984.

- [76] M. S. Turner and R. V. Wagoner. Gravitational radiation from slowly-rotating 'supernovae' - Preliminary results. In L. L. Smarr, editor, *Sources of Gravitational Radiation*, page 383, 1979.
- [77] K. A. van Riper. *Astrophys. J.*, **221**, 304, 1978.
- [78] J. R. Wilson. *unpublished*, 1977.
- [79] E. Seidel and T. Moore. *Phys. Rev. D.*, **35**, 2287, 1987.
- [80] E. Seidel, E. S. Myra, and T. Moore. *Phys. Rev. D.*, **38**, 2349, 1988.
- [81] R. Epstein. *Astrophys. J.*, **223**, 1037, 1978.
- [82] M. S. Turner. *Nature*, **274**, 565, 1978.
- [83] C. D. Ott, A. Burrows, L. Dessart, and E. Livne. *Astrophys. J.*, **685**, 1069, 2008.
- [84] Erik Schnetter, Christian D. Ott, Gabrielle Allen, Peter Diener, Tom Goodale, Thomas Radke, Edward Seidel, and John Shalf. Cactus Framework: Black holes to gamma ray bursts. In David A. Bader, editor, *Petascale Computing: Algorithms and Applications*, chapter 24. Chapman & Hall/CRC Computational Science Series, 2007. URL <http://arxiv.org/abs/0707.1607>.
- [85] K. Kotake, N. Ohnishi, and S. Yamada. *Astrophys. J.*, **655**, 406, 2007.
- [86] K. Kotake, S. Yamada, and K. Sato. *Phys. Rev. D.*, **68(4)**, 044023, 2003.
- [87] K. Kotake, S. Yamada, K. Sato, K. Sumiyoshi, H. Ono, and H. Suzuki. *Phys. Rev. D.*, **69(12)**, 124004, 2004.
- [88] C.L. Fryer, D.E. Holz, and S.A. Hughes. *Astrophys. J.*, **565**, 430, 2002.
- [89] C. L. Fryer and A. Heger. *Astrophys. J.*, **541**, 1033, 2000.
- [90] M. Obergaulinger, M. A. Aloy, and E. Müller. *Astron. Astrophys.* , **450**, 1107, 2006.
- [91] L. S. Finn and C. R. Evans. *Astrophys. J.*, **351**, 588, 1990.
- [92] L. Blanchet, T. Damour, and G. Schaefer. *Mon. Not. Roy. Astron. Soc.* , **242**, 289, 1990.
- [93] A. Marek, H. Dimmelmeier, H.-T. Janka, E. Müller, and R. Buras. *Astron. Astrophys.* , **445**, 273, 2006.
- [94] B. Müller, H. Dimmelmeier, and E. Müller. *Astron. Astrophys.* , **489**, 301, 2008.
- [95] M. Rampp and H.-T. Janka. *Astron. Astrophys.* , **396**, 361, 2002.
- [96] S. Scheidegger, T. Fischer, S. C. Whitehouse, and M. Liebendörfer. *Astron. Astrophys.* , **490**, 231, 2008.
- [97] E. Müller, M. Rampp, R. Buras, H.-T. Janka, and D. H. Shoemaker. *Astrophys. J.*, **603**, 221, 2004.
- [98] A. Marek, H. T. Janka, and E. Müller. *Submitted to Astron. Astrophys.* , *arXiv 0808.4136 [astro-ph]*, 2008.
- [99] L. S. Shapiro and S. A. Teukolsky. *Black Holes, White Dwarfs and Neutron Stars*. John Wiley & Sons, New York U. S. A., 1983.
- [100] J. A. Isenberg. *International Journal of Modern Physics D*, **17**, 265, 2008.
- [101] J. R. Wilson, G. J. Mathews, and P. Marronetti. *Phys. Rev. D.*, **54**, 1317, 1996.
- [102] T. W. Baumgarte and S. L. Shapiro. *Phys. Rep.*, **376(2)**, 41, 2003.
- [103] W. Kley and G. Schäfer. *Phys. Rev. D.*, **60(2)**, 027501, 1999.
- [104] A. Garat and R. H. Price. *Phys. Rev. D.*, **61(12)**, 124011, 2000.
- [105] G. B. Cook, S. L. Shapiro, and S. A. Teukolsky. *Phys. Rev. D.*, **53**, 5533, 1996.
- [106] P. Cerdá-Durán, G. Faye, H. Dimmelmeier, J. A. Font, J. M. Ibáñez, E. Müller, and G. Schäfer. *Astron. Astrophys.* , **439**, 1033, 2005.
- [107] J. A. Font. *Liv. Rev. Rel.*, **11**, 7, 2008.
- [108] H. Dimmelmeier, C. D. Ott, A. Marek, and H.-T. Janka. *Phys. Rev. D.*, **78(6)**, 064056, 2008.
- [109] H. Dimmelmeier, C. D. Ott, H.-T. Janka, A. Marek, and E. Müller. *Phys. Rev. Lett.*, **98(25)**, 251101, 2007.
- [110] H. Dimmelmeier, J. A. Font, and E. Müller. *Astron. Astrophys.* , **388**, 917, 2002.
- [111] H. Dimmelmeier, J. Novak, J. A. Font, J. M. Ibáñez, and E. Müller. *Phys. Rev. D.*, **71(6)**, 064023, 2005.
- [112] H. Dimmelmeier, J. A. Font, and E. Müller. *Astron. Astrophys.* , **393**, 523, 2002.
- [113] P. Cerdá-Durán, J. A. Font, and H. Dimmelmeier. *Astron. Astrophys.* , **474**, 169, 2007.
- [114] P. Cerdá-Durán, J. A. Font, L. Antón, and E. Müller. *arXiv:0804.4572 [astro-ph]*, 2008.
- [115] C. D. Ott, H. Dimmelmeier, A. Marek, H.-T. Janka, B. Zink, I. Hawke, and E. Schnetter. *Class. Quant. Grav.*, **24**, 139, 2007.
- [116] M. Shibata and Y. Sekiguchi. *Phys. Rev. D*, **69(8)**, 084024, 2004.
- [117] M. Shibata, Y. T. Liu, S. L. Shapiro, and B. C. Stephens. *Phys. Rev. D.*, **74(10)**, 104026, 2006.
- [118] M. Shibata and Y.-I. Sekiguchi. *Phys. Rev. D.*, **71(2)**, 024014, 2005.
- [119] C. D. Ott, H. Dimmelmeier, A. Marek, H.-T. Janka, I. Hawke, B. Zink, and E. Schnetter. *Phys. Rev. Lett.*, **98**, 261101, 2007.

- [120] M. Shibata and T. Nakamura. *Phys. Rev. D*, **52**, 5428, 1995.
- [121] T. W. Baumgarte and S. L. Shapiro. *Phys. Rev. D*, **59**, 024007, 1999.
- [122] A. Nagar and L. Rezzolla. *Class. Quant. Grav.*, **22**, 167, 2005.
- [123] A. Burrows and J. Hayes. *Phys. Rev. Lett.*, **76**, 352, 1996.
- [124] E. Müller and H.-T. Janka. *Astron. Astrophys.*, **317**, 140, 1997.
- [125] M. Obergaulinger, M. A. Aloy, H. Dimmelmeier, and E. Müller. *Astron. Astrophys.*, **457**, 209, 2006.
- [126] URL http://www.mpa-garching.mpg.de/rel_hydro/wave_catalogue.shtml. MPA Garching Gravitational Wave Catalog.
- [127] E. Müller. *Astron. Astrophys.*, **114**, 53, 1982.
- [128] E. Müller and W. Hillebrandt. *Astron. Astrophys.*, **103**, 358, 1981.
- [129] S. Yamada and K. Sato. *Astrophys. J.*, **450**, 245, 1995.
- [130] P. Goldreich and S. V. Weber. *Astrophys. J.*, **238**, 991, 1980.
- [131] A. Yahlil. *Astrophys. J.*, **265**, 1047, 1983.
- [132] S. T. Shapiro and A. P. Lightman. *Astrophys. J.*, **207**, 263, 1976.
- [133] J. E. Tohline. *Astrophys. J.*, **285**, 721, 1984.
- [134] J. N. Imamura, B. K. Pickett, and R. H. Durisen. *Astrophys. J.*, **587**, 341, 2003.
- [135] H. Shen, H. Toki, K. Oyamatsu, and K. Sumiyoshi. *Nucl. Phys. A*, **637**, 435, 1998. URL <http://user.numazu-ct.ac.jp/~sumi/eos>.
- [136] H. Shen, H. Toki, K. Oyamatsu, and K. Sumiyoshi. *Prog. Th. Phys.*, **100**, 1013, 1998.
- [137] S. E. Woosley, A. Heger, and T. A. Weaver. *Rev. Mod. Phys.*, **74**, 1015, 2002.
- [138] A. Heger, N. Langer, and S. E. Woosley. *Astrophys. J.*, **528**, 368, 2000.
- [139] M. Liebendörfer. *Astrophys. J.*, **633**, 1042, 2005.
- [140] J. M. Lattimer and F. D. Swesty. *Nucl. Phys. A*, **535**, 331, 1991.
- [141] C. D. Ott, A. Burrows, T. A. Thompson, E. Livne, and R. Walder. *Astrophys. J. Suppl. Ser.*, **164**, 130, 2006.
- [142] A. Heger, S. E. Woosley, and H. C. Spruit. *Astrophys. J.*, **626**, 350, 2005.
- [143] A. Burrows and J. M. Lattimer. *Astrophys. J.*, **270**, 735, 1983.
- [144] S. E. Woosley and A. Heger. *Astrophys. J.*, **637**, 914, 2006.
- [145] S. Chandrasekhar. *Ellipsoidal Figures of Equilibrium*. Yale University Press, New Haven, USA, 1969. revised edition 1987.
- [146] N. Stergioulas. *Liv. Rev. Rel.*, **6**, 3, 2003.
- [147] M. Saijo, M. Shibata, T. W. Baumgarte, and S. L. Shapiro. *Astrophys. J.*, **548**, 919, 2001.
- [148] L. Baiotti, R. D. Pietri, G. M. Manca, and L. Rezzolla. *Phys. Rev. D.*, **75(4)**, 044023, 2007.
- [149] G. M. Manca, L. Baiotti, R. DePietri, and L. Rezzolla. *Class. Quant. Grav.*, **24**, 171, 2007.
- [150] M. Rampp, E. Müller, and M. Ruffert. *Astron. Astrophys.*, **332**, 969, 1998.
- [151] J. D. Brown. Rotational Instabilities in post-Collapse Stellar Cores. In *AIP Conf. Proc. 575: Astrophysical Sources for Ground-Based Gravitational Wave Detectors*, page 234, 2001.
- [152] L. Villain, J. A. Pons, P. Cerdá-Durán, and E.ourgoulhon. *Astron. Astrophys.*, **418**, 283, 2004.
- [153] D. Lai and S. L. Shapiro. *Astrophys. J.*, **442**, 259, 1995.
- [154] D. Lai. Secular Bar-Mode Evolution and Gravitational Waves from Neutron Stars. In J. M. Centrella, editor, *AIP Conf. Proc. 575: Astrophysical Sources for Ground-Based Gravitational Wave Detectors*, page 246, 2001.
- [155] URL <http://www.stellarcollapse.org/gwcatalog>. Ott et al. Gravitational Wave Catalog.
- [156] A. L. Watts, N. Andersson, and D. I. Jones. *Astrophys. J. Lett.*, **618**, L37, 2005.
- [157] M. Saijo and S. Yoshida. *Mon. Not. Roy. Astron. Soc.*, **368**, 1429, 2006.
- [158] J. M. Centrella, K. C. B. New, L. L. Lowe, and J. D. Brown. *Astrophys. J. Lett.*, **550**, L193, 2001.
- [159] M. Saijo, T. W. Baumgarte, and S. L. Shapiro. *Astrophys. J.*, **595**, 352, 2003.
- [160] M. Shibata, S. Karino, and Y. Eriguchi. *Mon. Not. Roy. Astron. Soc.*, **343**, 619, 2003.
- [161] S. Ou and J. E. Tohline. *Astrophys. J.*, **651**, 1068, 2006.
- [162] P. Cerdá-Durán, V. Quilis, and J. A. Font. *Comp. Phys. Comm.*, **177**, 288, 2007.
- [163] C. D. Ott, S. Ou, J. E. Tohline, and A. Burrows. *Astrophys. J.*, **625**, L119, 2005.
- [164] S. A. Balbus and J. F. Hawley. *Astrophys. J.*, **376**, 214, 1991.
- [165] S. Akiyama, J. C. Wheeler, D. L. Meier, and I. Lichtenstadt. *Astrophys. J.*, **584**, 954, 2003.
- [166] M. Herant, W. Benz, W. R. Hix, C. L. Fryer, and S. A. Colgate. *Astrophys. J.*, **435**, 339, 1994.
- [167] A. Burrows, J. Hayes, and B. A. Fryxell. *Astrophys. J.*, **450**, 830, 1995.
- [168] H.-T. Janka and E. Müller. *Astron. Astrophys.*, **306**, 167, 1996.

- [169] W. Keil, H.-T. Janka, and E. Müller. *Astrophys. J. Lett.*, **473**, L111, 1996.
- [170] A. Mezzacappa, A. C. Calder, S. W. Bruenn, J. M. Blondin, M. W. Guidry, M. R. Strayer, and A. S. Umar. *Astrophys. J.*, **495**, 911, 1998.
- [171] L. Dessart, A. Burrows, E. Livne, and C. D. Ott. *Astrophys. J.*, **645**, 534, 2006.
- [172] P. Ledoux. *Astrophys. J.*, **105**, 305, 1947.
- [173] A. S. Endal and S. Sofia. *Astrophys. J.*, **220**, 279, 1978.
- [174] T. Foglizzo, P. Galletti, L. Scheck, and H.-T. Janka. *Astrophys. J.*, **654**, 1006, 2007.
- [175] J. M. Blondin, A. Mezzacappa, and C. DeMarino. *Astrophys. J.*, **584**, 971, 2003.
- [176] J. M. Blondin and A. Mezzacappa. *Astrophys. J.*, **642**, 401, 2006.
- [177] W. Iwakami, K. Kotake, N. Ohnishi, S. Yamada, and K. Sawada. *Astrophys. J.*, **678**, 1207, 2008.
- [178] T. Yamasaki and T. Foglizzo. *Astrophys. J.*, **679**, 607, 2008.
- [179] C. L. Fryer, D. E. Holz, and S. A. Hughes. *Astrophys. J.*, **609**, 288, 2004.
- [180] E. Livne, A. Burrows, R. Walder, I. Lichtenstadt, and T. A. Thompson. *Astrophys. J.*, **609**, 277, 2004.
- [181] S. E. Woosley and T. A. Weaver. *Astrophys. J. Supp. Ser.*, **101**, 181, 1995.
- [182] T. A. Thompson, A. Burrows, and P. A. Pinto. *Astrophys. J.*, **592**, 434, 2003.
- [183] A. Burrows and B. A. Fryxell. *Science*, **258**, 430, 1992.
- [184] S. W. Bruenn and A. Mezzacappa. *Astrophys. J. Lett.*, **433**, L45, 1994.
- [185] F. D. Swesty and E. S. Myra. Advances in Multi-Dimensional Simulation of Core-Collapse Supernovae. In A. Mezzacappa and G. M. Fuller, editors, *Open Issues in Core Collapse Supernova Theory*, page 176, 2005.
- [186] D. Lai and P. Goldreich. *Astrophys. J.*, **535**, 402, 2000.
- [187] J. W. Murphy, A. Burrows, and A. Heger. *Astrophys. J.*, **615**, 460, 2004.
- [188] W. Hillebrandt and R. G. Wolff. Models of Type II Supernova Explosions. In W. D. Arnett and J. W. Truran, editors, *Nucleosynthesis : Challenges and New Developments*, page 131, 1985.
- [189] W. Keil, H.-T. Janka, and E. Müller. PhD thesis, Technische Universität München, Munich, Germany, 1997.
- [190] D. Shoemaker. *Private communication*, 2006.
- [191] É. É. Flanagan and S. A. Hughes. *Phys. Rev. D.*, **57**, 4535, 1998.
- [192] R. Buras, M. Rampp, H.-T. Janka, and K. Kifonidis. *Astron. Astrophys.*, **447**, 1049, 2006.
- [193] K. H. Lockitch and J. L. Friedman. *Astrophys. J.*, **521**, 764, 1999.
- [194] S. Chandrasekhar. *Astrophys. J.*, **161**, 561, 1970.
- [195] J. L. Friedman and B. F. Schutz. *Astrophys. J.*, **222**, 281, 1978.
- [196] N. Andersson. *Astrophys. J.*, **502**, 708, 1998.
- [197] L. Lindblom, B. J. Owen, and S. M. Morsink. *Phys. Rev. Lett.*, **80**, 4843, 1998.
- [198] P. Arras, E. E. Flanagan, S. M. Morsink, A. K. Schenk, S. A. Teukolsky, and I. Wasserman. *Astrophys. J.*, **591**, 1129–1151, 2003.
- [199] H. Dimmelmeier, N. Stergioulas, and J. A. Font. *Mon. Not. Roy. Astron. Soc.*, **368**, 1609, 2006.
- [200] S. Bernuzzi and A. Nagar. *Phys. Rev. D.*, **78(2)**, 024024, 2008.
- [201] P. N. McDermott, H. M. van Horn, and J. F. Scholl. *Astrophys. J.*, **268**, 837, 1983.
- [202] P. N. McDermott, H. M. van Horn, and C. J. Hansen. *Astrophys. J.*, **325**, 725, 1988.
- [203] L. S. Finn. *Mon. Not. Roy. Astron. Soc.*, **227**, 265, 1987.
- [204] A. Reisenegger and P. Goldreich. *Astrophys. J.*, **426**, 688, 1994.
- [205] V. Ferrari, G. Miniutti, and J. A. Pons. *Mon. Not. Roy. Astron. Soc.*, **342**, 629, 2003.
- [206] V. Ferrari, G. Miniutti, and J. A. Pons. *Class. Quant. Grav.*, **20**, 841, 2003.
- [207] V. Ferrari, L. Gualtieri, J. A. Pons, and A. Stavridis. *Mon. Not. Roy. Astron. Soc.*, **350**, 763, 2004.
- [208] V. Ferrari, L. Gualtieri, and J. A. Pons. *Class. Quant. Grav.*, **24**, 5093, 2007.
- [209] A. Passamonti, M. Bruni, L. Gualtieri, and C. F. Sopuerta. *Phys. Rev. D.*, **71(2)**, 024022, 2005.
- [210] A. Passamonti, N. Stergioulas, and A. Nagar. *Phys. Rev. D.*, **75**, 084038, 2007.
- [211] A. Passamonti, M. Bruni, L. Gualtieri, A. Nagar, and C. F. Sopuerta. *Phys. Rev. D.*, **73(8)**, 084010, 2006.
- [212] E. B. Abdikamalov, H. Dimmelmeier, L. Rezzolla, and J. C. Miller. *arXiv:0806.1700 [astro-ph]*, 2008.
- [213] N. Stergioulas, T. A. Apostolatos, and J. A. Font. *Mon. Not. Roy. Astron. Soc.*, **352**, 1089, 2004.
- [214] K. Nomoto and M.-A. Hashimoto. *Phys. Rep.*, **163**, 13, 1988.

- [215] L. Dessart, A. Burrows, C. D. Ott, E. Livne, S.-Y. Yoon, and N. Langer. *Astrophys. J.*, **644**, 1063, 2006.
- [216] V. B. Braginskii and K. S. Thorne. *Nature*, **327**, 123, 1987.
- [217] J. I. Castor. *Radiation Hydrodynamics*. Radiation Hydrodynamics, by John I. Castor, pp. 368. ISBN 0521833094. Cambridge, UK: Cambridge University Press, November 2004., 2004.
- [218] R. Walder, A. Burrows, C. D. Ott, E. Livne, I. Lichtenstadt, and M. Jarrah. *Astrophys. J.*, **626**, 317, 2005.
- [219] K. Kotake, S. Yamada, and K. Sato. *Astrophys. J.*, **595**, 304, 2003.
- [220] G. Bazan and D. Arnett. *Astrophys. J.*, **496**, 316, 1998.
- [221] C. A. Meakin. *Hydrodynamic Modeling of Massive Star Interiors*. PhD thesis, The University of Arizona, Tucson, Arizona, 2006.
- [222] C. A. Meakin and D. Arnett. *Astrophys. J. Lett.*, **637**, L53, 2006.
- [223] E. B. Segalis and A. Ori. *Phys. Rev. D.*, **64(6)**, 064018, 2001.
- [224] B. M. S. Hansen and E. S. Phinney. *Mon. Not. Roy. Astron. Soc.*, **291**, 569, 1997.
- [225] D. Lai. Neutron Star Kicks and Asymmetric Supernovae. In D. Blaschke, N. K. Glendenning, and A. Sedrakian, editors, *Physics of Neutron Star Interiors*, volume 578 of *Lecture Notes in Physics*, Berlin Springer Verlag, page 424, 2001.
- [226] C. L. Fryer. *Astrophys. J. Lett.*, **601**, L175, 2004.
- [227] A. Heger, C. L. Fryer, S. E. Woosley, N. Langer, and D. H. Hartmann. *Astrophys. J.*, **591**, 288, 2003.
- [228] K. Sumiyoshi, S. Yamada, H. Suzuki, and S. Chiba. *Phys. Rev. Lett.*, **97(9)**, 091101, 2006.
- [229] K. Sumiyoshi, S. Yamada, and H. Suzuki. *Astrophys. J.*, **667**, 382, 2007.
- [230] T. W. Baumgarte, S. L. Shapiro, and M. Shibata. *Astrophys. J. Lett.*, **528**, L29, 2000.
- [231] A. Burrows. *Astrophys. J.*, **334**, 891, 1988.
- [232] W. Zhang, S. E. Woosley, and A. Heger. *Astrophys. J.*, **679**, 639, 2008.
- [233] S. E. Woosley. *Astrophys. J.*, **405**, 273, 1993.
- [234] C. T. Cunningham, R. H. Price, and V. Moncrief. *Astrophys. J.*, **224**, 643, 1978.
- [235] C. T. Cunningham, R. H. Price, and V. Moncrief. *Astrophys. J.*, **230**, 870, 1979.
- [236] C. T. Cunningham, R. H. Price, and V. Moncrief. *Astrophys. J.*, **236**, 674, 1980.
- [237] E. Seidel. *Phys. Rev. D.*, **42**, 1884, 1990.
- [238] E. Seidel. *Phys. Rev. D.*, **44**, 950, 1991.
- [239] T. Harada, H. Iguchi, and M. Shibata. *Phys. Rev. D.*, **68(2)**, 024002, 2003.
- [240] E. Berti, V. Cardoso, and C. M. Will. *Phys. Rev. D*, **73**, 064030, 2006.
- [241] L. Baiotti, I. Hawke, L. Rezzolla, and E. Schnetter. *Phys. Rev. Lett.*, **94(13)**, 131101, 2005.
- [242] L. Baiotti, I. Hawke, and L. Rezzolla. *Class. Quant. Grav.*, **24**, 187, 2007.
- [243] B. et al. Abbott. *Class. Quant. Grav.*, **24**, 5343, 2007.
- [244] E. Berti and V. Cardoso. *Phys. Rev. D*, **74**, 104020, 2006.
- [245] T. Nakamura. *Prog. Theor. Phys.*, **65**, 1876, 1981.
- [246] R. F. Stark and T. Piran. *Phys. Rev. Lett.*, **55**, 891, 1985.
- [247] A. Nagar, O. Zanotti, J. A. Font, and L. Rezzolla. *Phys. Rev. D.*, **75(4)**, 044016, 2007.
- [248] N. Arnaud, M. Barsuglia, M.-A. Bizouard, V. Brisson, F. Cavalier, M. Davier, P. Hello, S. Kreckelbergh, and E. K. Porter. *Astropart. Phys.*, **21**, 201, 2004.
- [249] E. Katsavounidis. *private communication*, 2008.
- [250] A. V. Filippenko. *Ann. Rev. Astron. Astrophys.*, **35**, 309, 1997.
- [251] L. A. G. Monard. *Central Bureau Electronic Telegrams CBET*, 1315, 2008.
- [252] I. D. Karachentsev, V. E. Karachentseva, W. K. Huchtmeier, and D. I. Makarov. *Astron. J.*, **127**, 2031, 2004.
- [253] C. Jacques and E. Pimentel. *Central Bureau for Astronomical Telegrams, IAU*, 8482, 2005.
- [254] S. Nakana. *Central Bureau for Astronomical Telegrams, IAU*, 8377, 2004.
- [255] D. Singer, H. Pugh, and W. Li. *Central Bureau for Astronomical Telegrams, IAU*, 8297, 2004.
- [256] I. D. Karachentsev, A. E. Dolphin, D. Geisler, E. K. Grebel, P. Guhathakurta, P. W. Hodge, V. E. Karachentseva, A. Sarajedini, P. Seitzer, and M. E. Sharina. *Astron. Astrophys.*, **383**, 125, 2002.
- [257] W. Schwartz and W. Li. *Central Bureau for Astronomical Telegrams, IAU*, 8051, 2004.
- [258] D. Maoz and F. Mannucci. *The Astronomer's Telegram*, 1464, 2008.
- [259] S. Mattila, S. J. Smartt, J. J. Eldridge, J. R. Maund, R. M. Crockett, and I. J. Danziger. *Submitted to ApJL, arXiv:0809.0206 [astro-ph]*, 2008.
- [260] M. Landry. *Private communication*, 2008.
- [261] T. Z. Summerscales, A. Burrows, L. S. Finn, and C. D. Ott. *Astrophys. J.*, **678**, 1142, 2008.
- [262] P. R. Brady and S. Ray-Majumder. *Class. Quant. Grav.*, **21**, 1839, 2004.
- [263] J. C. Wheeler and S. Akiyama. *Astrophys. J.*, **654**, 429, 2007.
- [264] URL <http://www.astro.cardiff.ac.uk/geo/euro>. EURO.